A "Moonlighting" Dizinc Aminopeptidase from *Streptomyces griseus*: Mechanisms for Peptide Hydrolysis and the 4×10^{10}-Fold Acceleration of the Alternative Phosphodiester Hydrolysis[†]

Altan Ercan,[‡] Hyun Ik Park,[§] and Li-June Ming*

Department of Chemistry and Institute for Biomolecular Science, University of South Florida, 4202 East Fowler Avenue, CHE205, Tampa, Florida 33620-5250

ABSTRACT: A unique "enzyme catalytic promiscuity" has recently been observed, wherein a phosphodiester and a phosphonate ester are hydrolyzed by a dinuclear aminopeptidase and its metal derivatives from *Streptomyces griseus* (*Sg*AP) [Park, H. I., Ming, L.-J. (1999) *Angew. Chem., Int. Ed. Engl. 38*, 2914−2916 and Ercan, A., Park, H. I., Ming, L.-J. (2000) *Chem. Commun.* 2501−2502]. Because tetrahedral phosphocenters often serve as transition-state inhibitors toward the hydrolysis of the peptide, phosphoester hydrolysis by peptidases is thus not expected to occur effectively and must take place through a unique mechanism. Owing to the very different structures and mechanistic requirements between phosphoesters and peptides during hydrolysis, the study of this effective phosphodiester hydrolysis by *Sg*AP may provide further insight into the action of this enzyme *that is otherwise not obtainable from regular peptide substrates*. We present herein a detailed investigation of both peptide and phosphodiester hydrolyses catalyzed by *Sg*AP. The latter exhibits a first-order rate enhancement of 4×10^{10}-fold compared to the uncatalyzed reaction at pH 7.0 and 25 °C. The results suggest that peptide and phosphodiester hydrolyses by *Sg*AP may share a common reaction mechanism to a certain extent. However, their differences in pH dependence, phosphate and fluoride inhibition patterns, and proton inventory reflect that they must follow different pathways. Mechanisms for the two hydrolyses are drawn on the basis of the results, which provide the foundation for further investigation of the catalytic promiscuity of this enzyme by means of physical and molecular biology methods. The catalytic versatility of *Sg*AP suggests that this enzyme may serve as a unique "natural model system" for further investigation of dinuclear hydrolysis. A better understanding of enzyme catalytic promiscuity is also expected to shed light on the evolution and action of enzymes.

Enzymes evolve to act on a specific substrate or group of analogous substrates via stabilization of the transition state $(TS^{\ddagger})^1$ of the substrates to enhance the reaction rate (*1*, *2*). Consequently, $TS^{\ddagger}$ analogues often serve as inhibitors for the corresponding enzymes. The concept of $TS^{\ddagger}$ recognition in enzyme catalysis is also illustrated in the action of catalytic antibodies induced by haptens that resemble the $TS^{\ddagger}$s in the corresponding reactions (*3*, *4*). In enzymatic hydrolyses of peptide, ester, and amide, the *gem*-diolate-like $TS^{\ddagger}$ can be mimicked by the tetrahedral phosphocenter of phosphoesters, phosphonates, and phosphoamidates that are known to inhibit

the corresponding hydrolases (*5*−*12*). The mechanisms for hydrolyses of phosphoesters and peptides are quite different, i.e., nucleophilic attack from above or below the $>C=O$ plane to form a tetrahedral $TS^{\ddagger}$ in peptide hydrolysis but an "in-line" S_N2-like attack from the opposite site of the leaving group to form a trigonal bipyramidal $TS^{\ddagger}$ in phosphoester hydrolysis (*13*, *14*). Accordingly, each class of hydrolytic enzymes should perform only one type of hydrolysis, despite the presence of a highly activated nucleophile, such as a water molecule, in the active site ready for nucleophilic attack at the scissile bond of the substrates.

Recently, a dinuclear aminopeptidase and its metal derivatives from *Streptomyces griseus* (*Sg*AP) were observed to exhibit an unexpected "enzyme catalytic promiscuity" (*15*−*19*), wherein the phosphodiester bis(*p*-nitrophenyl)phosphate (*20*) and the phosphonate ester *p*-nitrophenyl phenylphosphonate (*21*) were hydrolyzed with enormous rate accelerations compared to the rates of the uncatalyzed reactions. Incidentally, the dinuclear prolidase from *Alteromonas* species was also discovered to exhibit alternative activities toward the hydrolysis of phosphoester and phosphofluorinate bonds in nerve agents such as sarin and soman (*22*−*24*). Because phosphoesters are analogous to the $TS^{\ddagger}$ of peptides during hydrolysis, how a phosphoester is recognized and how

1 Abbreviations: ABP, 1-aminobutylphosphonate; AEP, 1-aminoethylphosphonate; AP, aminopeptidase; *Ap*AP, *Aeromonas proteolytica* AP; blAP, bovine lens AP; BNPP, bis(*p*-nitrophenyl)phosphate; EI, enzyme−inhibitor; ES, enzyme−substrate; ESI, enzyme−substrate−inhibitor; NMR, nuclear magnetic resonance; NPP, *p*-nitrophenylphosphate; *p*NA, *p*-nitroanilide; *Sg*AP, *Streptomyces griseus* AP; TS‡, transition state.
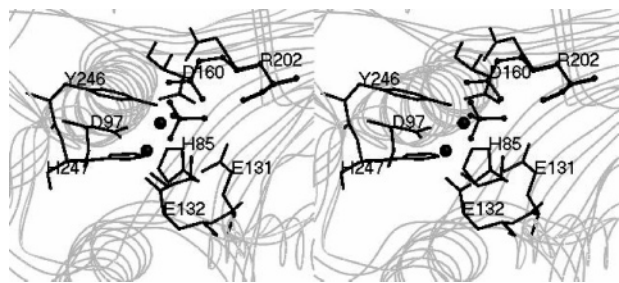
FIGURE 1: Structure of the active site of *Sg*AP (PDB 1XJO). The "bound phosphate" and the three auxiliary amino acid side chains (Tyr246, Glu131, and Arg202) that are presumably involved in *Sg*AP catalysis are shown. The side chain of Arg202 is not revealed in the original crystal structure, which has been added to show an extended configuration (line structure), and can easily adopt a configuration with the guanidinium group close to the "bound phosphate".

its trigonal bipyramidal TS‡ is stabilized by a peptidase present challenging mechanistic questions. These two dinuclear metallohydrolases can thus be introduced as unique "*natural* model systems" and serve as counterparts of those widely studied "*synthetic* model systems" (*25−31*) to offer a rare opportunity for the investigation of the mechanistically different peptide and phosphoester hydrolyses in one active site.

Metal-centered enzymatic (*32−41*) and nonenzymatic (*25−31*) hydrolyses of peptides and phosphodiesters have been extensively studied in recent years, wherein the ionization constant of a coordinated water is dramatically decreased by $>10^8$-fold from pK_a = 15.74 to $\sim$7 or lower by the metal ion(s) to produce a nucleophilic hydroxide. This process dramatically enhances the local concentration of OH$^-$ in the active site to render hydrolysis possible at neutral or lower pH. In the meantime, the binding of the substrate to the metal(s) further polarizes the scissile bond, making nucleophilic attack more effective. One significant difference between enzymatic and nonenzymatic catalysis is the presence of specific recognition in the former case, which renders catalytic conversion of only one type of substrate, e.g., peptide hydrolysis by proteases and phosphoester hydrolysis by phosphoesterases and nucleases.

Several metallohydrolases have been characterized by means of X-ray crystallography to contain a dinuclear catalytic center (*32−36, 41*), including *Sg*AP (*42−44*), those aminopeptidases (APs) from *Aeromonas proteolytica* (*Ap*AP) (*45−47*), bovine lens (blAP) (*48, 49*), and *Escherichia coli* (*50*), aminopeptidase P from *E. coli* (*51, 52*), and prolidase from *Pyrococcus* (*53*). The two zinc ions in *Sg*AP are coordinated by the side chains of His, Asp, and Glu, separated by 3.6 Å, and bridged by the carboxylate of Asp97 (Figure 1). A bridging tetrahedral electron density in *Sg*AP was suggested to be a dibasic phosphate (*42−44*), which was thought to replace the bridging hydroxide found in other dinuclear APs (*42*). One of the phosphate oxygen atoms bridges the two zinc ions, and another one coordinates to only one zinc. This binding pattern resembles that of the bound TS‡ inhibitors leucinal and leucine phosphonic acid in blAP (*48, 49*). However, phosphate was concluded not to bind to the metal ions in recent kinetic (*54*) and ^{31}P nuclear magnetic resonance (NMR) relaxation studies (*55*), reflecting that differences may exist between solution and solid states of *Sg*AP. The mechanism of dinuclear APs has emerged from

recent kinetic, spectroscopic, and crystallographic studies (*42−50, 56−58*), wherein the N-terminal amino group of the substrate is bound to an active-site metal or a side chain and the scissile carbonyl group is also bound to a metal and then followed by nucleophilic attack by either a terminal or bridging hydroxide. Whether or not the catalytic promiscuity of *Sg*AP toward phosphodiester hydrolysis follows the same reaction pathway as peptide hydrolysis cannot be concluded from the previous studies. We report herein a further investigation of the normal peptide hydrolysis and the catalytic promiscuity toward phosphodiester hydrolysis by *Sg*AP. The mechanisms for these two hydrolyses are proposed on the basis of the results from the investigation, which provide the foundation for future research of the catalytic promiscuity of this enzyme by means of physical and molecular biology methods. Moreover, the exploration of enzyme catalytic promiscuity is expected to provide further information about the evolution and action of enzymes (*15−19*).

MATERIALS AND METHODS

Preparation of Native, Apo, and Modified SgAP. *Sg*AP was prepared from Pronase (Sigma-Aldrich and Fluka, St. Louis, MO) according to the published procedures, wherein the first eluted active fractions from the final (diethylamino)-ethyl (DEAE) column was used for this study and the concentration was determined according to $E^{1\%}_{280} = 15$ or from stoichiometric metal-ion titration with standard Zn^{2+} or Co^{2+} solution (*59, 60*). The native Zn^{2+} was removed from *Sg*AP with 1,10-phenanthroline via dialysis (*59, 61*). Arg-specific modification of *Sg*AP with phenylglyoxal was carried out according to published procedures (*55*). *Ap*AP with an activity of 117 units/mg was purchased from Sigma-Aldrich. All containers were treated with ethylenediaminetetraacetic acid (EDTA) solution and rinsed with deionized water (18 MΩ; Milli-Q, Fisher Scientific, Fairlawn, NJ) prior to use.

Assay and Kinetic Studies. The substrates Leu-*p*-nitroanilide (Leu-*p*NA), *p*NA derivatives of other amino acids, and bis(*p*-nitrophenyl)phosphate (BNPP) and the inhibitors were purchased from Sigma-Aldrich. Enzyme activities were determined according to the increase in absorbance at 405 nm because of the release of *p*-nitroaniline (10 150 M^{-1} cm^{-1}) or *p*-nitrophenol (17 500 M^{-1} cm^{-1}) in 0.10 M *N*-2-hydroxyethylpiperazine-*N'*-2-ethanesulfonic acid (HEPES) buffers at pH 8.0 and 30 °C in the presence of a saturating amount of Ca^{2+} (i.e., 10 mM below pH 6.5 and 2 mM above pH 6.5) on a Cary 3E or Cary 50 spectrophotometer (Varian, Palo Alto, CA). Inhibitions were performed with two to three different inhibitor concentrations under the above conditions. The kinetic parameters k_{cat} and K_m were obtained by nonlinear regression fitting of the data directly to the Michaelis−Menten equation, and the type of inhibition was determined accordingly. The activity of *Ap*AP was measured similarly. The rate constants for uncatalyzed hydrolysis of Gly-, Val-, Lys-, Met-, and Leu-*p*NA substrates are (2.49 ± 0.05, 2.08 ± 0.05, 2.50 ± 0.01, 4.06 ± 0.08, and 9.80 ± 0.07) × 10^{-8} s^{-1}, respectively, determined from the slope of the corresponding rate−concentration plots.

The molar absorptivity of *p*-nitrophenol varies with pH, which was determined to be 1930, 4220, 9330, 14 500,

17 500, 18 700, 19 100, 19 300, and 19 400 (with standard deviations in the range of 5−30) M^{-1} cm^{-1} at pH 6.0, 6.5, 7.0, 7.5, 8.0, 8.5, 9.0, 9.5, and above 10.0, respectively, whereas that of 4-nitroaniline was constant within the pH range. The buffers at 20 mM used for different pH regions were acetate at pH 4.5−5.0, 2-(*N*-morpholino)ethanesulfonic acid (MES) at pH 5.5−6.5, HEPES at pH 7.0−8.0, tris-aminopropanesulfonic acid (TAPS) at pH 8.5−9.5, and 3-(cyclohexylamino)-1-propanesulfonic acid (CAPS) at pH 10.0. These buffers have no observable effect on the reaction rate under the experimental conditions. Owing to the low molar absorptivity of 4-nitrophenol at pH < 6.0, the rates of BNPP hydrolysis at low pH values were determined by quenching a 1.0 mL reaction mixture and a control separately with 1.0 mL of 1.0 M NaOH after 10 min of incubation and then their absorption difference at 405 nm was determined.

pH Dependence. The ionization constants for the general base and general acid involved in catalyses can be obtained by nonlinear fitting of the rate constants to a two-deprotonation process with respect to pH according to eq 1 (*62, 63*)

$$k_{obs} = k_{lim} / \left\{ \left(1 + \frac{[H^+]}{K_{a1}}\right)\left(1 + \frac{K_{a2}}{[H^+]}\right) \right\} \quad (1)$$

where k_{obs} is the observed rate constant (k_{cat} or k_{cat}/K_m), k_{lim} is the pH-independent limiting rate constant, and K_a values are the ionization constants. Analogous fitting can be performed in case more than two ionization steps are observed (*62−64*). Direct pH titrations (Radiometer PHM 290 pH-Stat, Radiometer, Westlake, OH) reveal the pK_a values of the amino group of Leu-, Lys-, and Met-*p*NA to be 7.94 ± 0.03, 6.83 ± 0.05, and 6.95 ± 0.03, respectively. The low pK_a values are attributable to the strong electron-withdrawing *p*NA functionality on the substrates.

Solvent Isotope Effect. Proton inventory studies (*65*) were performed at 20 °C in 50 mM HEPES buffer at pH/pD 8.0 containing 2 mM $CaCl_2$ under different deuterium atom fractions (*n*). The kinetic constants k_{cat} and k_{cat}/K_m at different *n* values were fitted to the simplified version of the Gross−Butler equations for one- (eq 2) or two-proton transfer (eq 3 or eq 4 when the two proton transfers are indistinguishable) at the rate-determining step, in which k_n is the measured rate constant at *n*, k_0 is the rate constant in H_2O, and k_H/k_D is the kinetic isotope effect, which can be obtained from the fitting. Multi-proton-transfer processes are expressed in the form of eq 5. However, the different processes in the multi-proton-transfer case usually cannot be specifically defined and distinguished from each other.

$$k_n = k_0[1 - n + n/(k_H/k_D)] \quad (2)$$

$$k_n = k_0[1 - n + n/(k_H/k_D)_1][1 - n + n/(k_H/k_D)_2] \quad (3)$$

$$k_n = k_0[1 - n + n/(k_H/k_D)]^2 \quad (4)$$

$$k_n = k_0(k_H/k_D)^n \quad (5)$$

Influence of Viscosity. The influence of viscosity on the activity of the enzyme is checked by the use of sucrose as the viscosogenic agent (at 16, 23, 30, and 35% w/v) in 20 mM HEPES buffer at pH 8.0 and 30 °C in the presence of 0.1 M NaCl and 10 mM $CaCl_2$. The rate constant for the

enzymatic reaction is inversely proportional to the relative microviscosity (solution versus solvent) in the form of eq 6, if diffusion plays a role in the enzyme kinetics (*66, 67*), in which the rate constant *k* values are defined in the Michaelis−Menten equation, the superscript denotes the constants without the viscosogen, and η/η_0 is the relative viscosity. This equation can be expressed in the form of a normalized plot (eq 7), where $P = k_{-1}^0/k_{cat}$. If the reaction is insensitive to viscosity, the slope in the plot is 0; if the reaction is viscosity-controlled, the slope in the plot is 1 (*66, 67*).

$$1/\frac{k_{cat}}{K_M} = \frac{1}{k_1^0}\left(\frac{\eta}{\eta_0}\right) + \frac{k_{-1}^0}{k_1^0 k_{cat}} \quad (6)$$

$$\left(\frac{k_{cat}}{K_M}\right)^0 / \left(\frac{k_{cat}}{K_M}\right) = \frac{P}{1+P} + \frac{1}{1+P}\left(\frac{\eta}{\eta_0}\right) \quad (7)$$

Temperature Dependence. *Sg*AP is quite resistant to denaturation by heat (*59*), which allows kinetic measurements to be performed up to 60 °C. The rates of enzyme-catalyzed hydrolysis of the different substrates in 0.1 M HEPES at pH 8.0 in the presence of 2 mM Ca^{2+} were measured at five different temperatures from 20 to 60 °C. The initial rate of hydrolysis at 60 °C is linear in the experimental time duration. The activation energy E_a for each substrate was obtained by fitting k_{cat} with respect to temperature to the Arrhenius equation, from which $\Delta H^{\ddagger}$ is obtained. $\Delta G^{\ddagger}$ is calculated from k_{cat}, and $\Delta S^{\ddagger}$ can be calculated from the other two parameters. The pK_a values from the activity−pH profile of Leu-*p*NA hydrolysis by *Sg*AP were determined at five different temperatures, and the heat of ionization ΔH_{ion} for the pK_a can be obtained from the slope of the line ($\Delta H_{ion}/2.303R$) according to the van't Hoff equation.

Modeling of Substrate Binding. The peptide substrate is modeled into the active site by the use of the crystal structure of the enzyme-bound $TS^{\ddagger}$ analogue (*8*) or product (*44*) as a template. The substrate is superimposed onto the $TS^{\ddagger}$ analogue by the use of the canned program from BioMed-CAChe 6.1.10 (Fujitsu, Beaverton, OR) with two different orientations to render the terminal water that is hydrogen-bonded to Tyr246 or the bridging water as the nucleophile. In the case of BNPP hydrolysis, the phosphocenter is superimposed onto either the peptide resulted from the above or the enzyme-bound $TS^{\ddagger}$ analogue (*8*), which renders the terminal water that is hydrogen-bonded to Tyr246 or the water in place of the coordinated amino group as the nucleophile, respectively. ViewerLite 5.0 (Accelrys, San Diego, CA) was used for displaying the structures.

RESULTS

Peptide and BNPP Hydrolyses by SgAP. *Sg*AP is active toward various peptides with different N-terminal side chains (Table 1) and specific toward hydrophobic ones (*59−61*). Moreover, *Sg*AP also exhibits a significant activity toward the hydrolysis of the phosphodiester BNPP with $k_{cat} = 0.42$ s^{-1} and $k_{cat}/K_m = 124$ M^{-1} s^{-1} at pH 8.0, consistent with previous observations (*20*). However, the phosphomonoester *p*-nitrophenylphosphate (NPP) is not hydrolyzed by *Sg*AP under the same conditions (*21*) and is an inhibitor (Table 2). Phosphoesters resemble the *gem*-diolate $TS^{\ddagger}$ of peptides during hydrolysis and are known inhibitors for esterases,

Table 1: Kinetic and Thermodynamic Parameters for the Hydrolysis of Amino Acid-*p*NA Substrates and BNPP by *Sg*AP[a]

amino acid-*p*NA	Leu	Met	Val	Ala	Lys	Gly	BNPP
k_{cat} (s^{-1})	657 ± 54	43.3 ± 1.4	0.28 ± 0.02	4.9 ± 0.5	2.8 ± 0.5	1.1 ± 0.3	0.42 ± 0.01
K_m (mM)	0.45 ± 0.04	0.58 ± 0.08	0.18 ± 0.05	7.8 ± 0.8	5.0 ± 0.4	1.4 ± 0.3	3.4 ± 0.2
k_{cat}/K_m (M^{-1} s^{-1})	(1.5 ± 0.2) × 10^6	(7.5 ± 1.1) × 10^5	1600 ± 500	630 ± 90	560 ± 110	760 ± 260	124 ± 8
E_a (kJ/mol)	42 ± 2	30 ± 1	48 ± 2	42 ± 1	51 ± 1	57 ± 1	38 ± 1
$\Delta H^\ddagger$ (kJ/mol)[b]	39 ± 2	28 ± 1	46 ± 2	39 ± 1	49 ± 1	55 ± 1	35 ± 1
$\Delta S^\ddagger$ (J/Kmol)[b]	−62 ± 7	−120 ± 3	−110 ± 7	−100 ± 4	−76 ± 4	−64 ± 4	−140 ± 3
$\Delta G^\ddagger$ (kJ/mol)	58.1 ± 0.4	64.8 ± 0.1	77.5 ± 0.2	70.3 ± 0.3	71.7 ± 0.5	74.1 ± 0.7	76.4 ± 0.0
RE[c] (10^9)	6.70	1.07	0.0135		0.112	0.0274	38.5[d]

[a] A total of 0.1 M HEPES buffer at pH 8.0 and 30 °C in the presence of 10 mM Ca^{2+} and 100 mM NaCl. [b] Autohydrolyses of Leu-*p*NA, Gly-*p*NA, and BNPP at pH 8.0 and 30 °C yield $\Delta H^\ddagger$ = 69.1, 84.9, and 87.7 kJ/mol and $\Delta S^\ddagger$ = −151, −107, and −115 J K^{-1} mol^{-1}, respectively. [c] Rate enhancement or catalytic proficiency in terms of the first-order rate constant (*91*) k_{cat}/k_0. The observed rate constants for nonenzymatic hydrolysis were determined to be 9.8 × 10^{-8}, 3.9 × 10^{-8}, 2.1 × 10^{-8}, 4.1 × 10^{-8}, and 2.5 × 10^{-8} s^{-1} for Leu-, Gly-, Val-, Met-, and Lys-*p*NA, respectively. [d] The catalytic proficiency at pH 7.0, considering OH$^-$ being the nucleophile in autohydrolysis.

Table 2: Inhibition Toward *Sg*AP Catalysis[a]

	K_i (mM)			K_i (mM)	
inhibitors	Leu-*p*NA	BNPP	inhibitors	Leu-*p*NA	BNPP
bestatin	(1.5 ± 0.3) × 10^{-3} (2.0 ± 0.3)[b] × 10^{-3} (1.2 ± 0.1)[c] × 10^{-3}	(1.30 ± 0.04) × 10^{-3}	Leu-amide *R*-leucinol	1.72 ± 0.05 2.7 ± 0.1	1.72 ± 0.06 5.1 ± 0.2
ABP[d]	(2.0 ± 0.1) × 10^{-3} (1.9 ± 0.2)[b] × 10^{-3} (1.9 ± 0.1)[c] × 10^{-3}	(2.2 ± 0.1) × 10^{-3}	*S*-leucinol NPP[d]	3.0 ± 0.1 0.94 ± 0.04	3.6 ± 0.3 0.84 ± 0.03
R-AEP[d]	0.70 ± 0.03	0.71 ± 0.07	BNPP	5.10 ± 0.08	4.5 ± 0.2[e]
S-AEP[d]	1.3 ± 0.1	1.0 ± 0.1	BNPP (*Ap*AP[f])	8.1 ± 1.1	
Leu-NHOH	0.038 ± 0.002 0.052 ± 0.005[b] 0.031 ± 0.006[c]	0.040 ± 0.010	P$_i$[d] (pH 6.0)[g] P$_i$[d] (pH 8.0)[i]	0.75[h] 30[h]	2.4 ± 0.3[h] 25 ± 13[h]
Ile-NHOH	0.017 ± 0.001	0.023 ± 0.002	fluoride	21[j]	240 ± 50[k]
Lys-NHOH	2.6 ± 0.4	1.6 ± 0.1			

[a] All of the assays were performed toward Leu-*p*NA hydrolysis in 0.1 M HEPES buffer at pH 8.0 in the presence of 10 mM Ca^{2+} ion, except those indicated. All of the inhibitors, except phosphate and fluoride, exhibit a competitive inhibition pattern. [b] Lys-*p*NA is the substrate. [c] Ala-*p*NA is the substrate. [d] ABP, 1-aminobutylphophonate; AEP, 1-aminoethylphophonate; NPP, *p*-nitrophenylphosphate; P$_i$, inorganic phosphate. [e] K_m value for BNPP hydrolysis by *Sg*AP. [f] Inhibition against *Ap*AP toward Leu-*p*NA hydrolysis at pH 8.0. [g] P$_i$ is a very weak competitive inhibitor toward Leu-*p*NA hydrolysis by *Ap*AP at pH 6.0 (*55*) (K_i = 120 mM, estimated at 0.4 M phosphate). [h] P$_i$ is a noncompetitive inhibitor toward peptide hydrolysis (*54, 55*) but a competitive inhibitor toward BNPP hydrolysis. [i] P$_i$ is not an inhibitor (up to 0.93 M) toward Leu-*p*NA hydrolysis by *Ap*AP at pH 8.0. [j] Fluoride is an uncompetitive inhibitor toward Leu-*p*NA hydrolysis (*54*). [k] Dissociation constant K_d for the *activation* of BNPP hydrolysis at pH 8.0. Cl$^-$ and I$^-$ are very weak activators, with K_d estimated to be 1.6 and 11 M at pH 8.0.

amidases, and peptidases (*5−12*). Thus, it is very interesting that BNPP can be effectively hydrolyzed by the peptidase *Sg*AP.

The thermostability of *Sg*AP allows its k_{cat} to be obtained between 20 and 60 °C to yield the activation energy E_a and other thermodynamic parameters of activation (Figure 2A). The heat of activation $\Delta H^\ddagger$ in the hydrolysis of BNPP by *Sg*AP is close to those in the hydrolysis of Leu-, Met-, Val-, and Ala-*p*NA by *Sg*AP, wherein the $-\Delta S^\ddagger$ value in the hydrolysis of BNPP exhibits the largest magnitude (Table 1). Lys-*p*NA has a higher $\Delta H^\ddagger$ value than other substrates, which can be reasonably explained by the involvement of dehydration of the amino group on the side chain in the activation process (*68*). The large $\Delta H^\ddagger$ value for Gly-*p*NA hydrolysis may be attributable to the lack of a specific interaction to stabilize the TS‡ during catalysis.

Inhibition of SgAP toward the Hydrolyses of Peptides and BNPP. Because *Sg*AP has a high specificity toward hydrophobic N-terminal amino acids (*61*), it can be inhibited by hydrophobic AP inhibitors, such as the TS‡-mimicking bestatin (*69, 70*) and ±-aminobutylphosphonate (*71*) and metal-chelating hydroxamates (*72*) (Table 2). The same inhibition pattern and similar K_i values of an inhibitor toward different substrates (Table 2) reflect that the inhibitor is
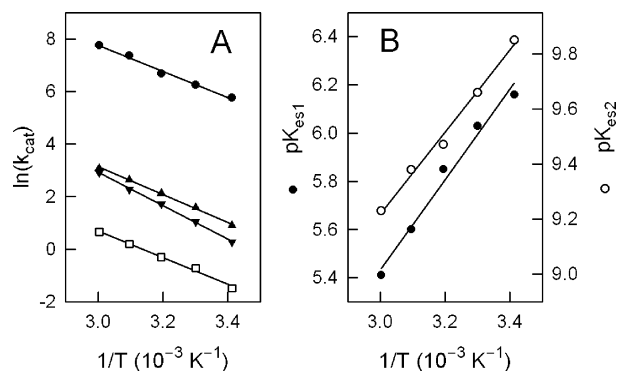

FIGURE 2: (A) Temperature dependence of k_{cat} for the hydrolysis of Leu-, Ala-, and Lys-*p*NA and BNPP (from top to bottom) by *Sg*AP, in which the activation energy (E_a) is obtained by direct fitting to the Arrhenius equation. (B) Temperature dependence of pK_a values of Leu-*p*NA hydrolysis by *Sg*AP obtained from activity− pH profiles (cf. Figure 4A). The ΔH_{ion} values for pK_{es1} and pK_{es2} are obtained from the slope of the line ($\Delta H_{ion}/2.303R$) according to the van't Hoff equation.

bound to the same site during catalyses of the different substrates and the different substrates may be recognized and hydrolyzed by *Sg*AP in a similar fashion, despite their very different structures.
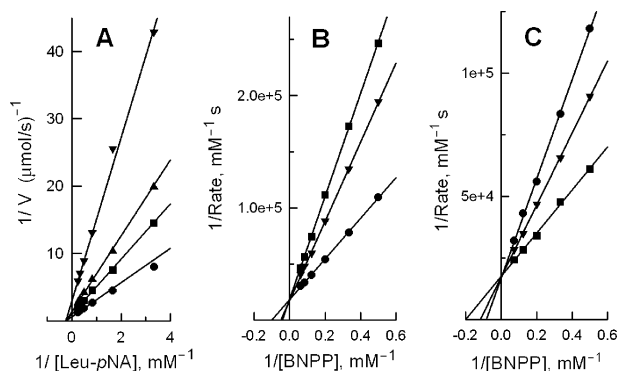
FIGURE 3: Phosphate inhibition of ZnZn-*Sg*AP toward the hydrolysis of (A) Leu-*p*NA at pH 7.4 with phosphate concentrations at 0.0, 5.0, 20, and 50 mM (from bottom to top) and (B) BNPP at pH 8.0 with phosphate concentrations at 0, 32, and 74 mM (from bottom to top). (C) F⁻ activation toward BNPP hydrolysis at pH 8.0 by ZnZn-*Sg*AP at NaF concentrations of 0.00, 0.10, and 0.30 M (from top to bottom).

FIGURE 4: pH profiles of (A and E) k_{cat}, (B and F) k_{cat}/K_m, and (C and G) pK_m toward the hydrolysis of Leu-*p*NA and BNPP, respectively, by *Sg*AP (●) and phenylglyoxal-modified *Sg*AP (▲). The pH profiles of the inhibition constant of L-Leu (▲, D) and 1-aminobutyl phosphonates (●, D) toward the hydrolysis of Leu-*p*NA by *Sg*AP in 0.1 M buffers, 10 mM Ca²⁺, and 10 µM Zn²⁺. The dashed curve in D represents the deprotonation of Leu. (H) pH profile of K_i of phosphate inhibition toward the hydrolysis of BNPP by *Sg*AP fitted with a single-ionization process (···) and a two-ionization process (—). All of the fittings were obtained with nonlinear regression, wherein C, D, G, and H are displayed as linear plots.

The inhibition constants for leucinamide and leucinol are similar, suggesting similar interactions of these two inhibitors in the enzyme−inhibitor (EI) complex, which may be attributed to the binding of the amino-isobutyl group and the carbonyl/hydroxyl oxygen to the active-site metals. Changing the hydrophobic group from a propyl in 1-aminobutylphosphonate (ABP) and a benzyl group in bestatin to a methyl in 1-aminoethylphosphonate (AEP) significantly decreases the inhibition by 370−860-fold (Table 2), corresponding to a difference in free energy of 14.7−16.7 kJ/mol at 25 °C, which is more than a regular London dispersion force (in a magnitude of only about 0.2 kJ/mol at a distance of 0.5 nm; *73*) for molecular interactions. A change from a TS‡-like configuration in bestatin and ABP to leucinamide and leucinol decrease the inhibition by ∼1500-fold (Table 2), corresponding to 18 kJ/mol, close to an average energy of a hydrogen bond. Moreover, Lys-NHOH is about 2 orders less efficient than Leu- and Ile-NHOH, despite their similar metal-binding motif. These observations reflect the importance of hydrophobic recognition and possible involvement of a hydrogen-bonding interaction at the TS‡ in the action of *Sg*AP.

Influences by Phosphate and Halide. Phosphate was found to be a *pure noncompetitive inhibitor* toward peptide hydrolysis by *Sg*AP at pH 5.5−9.0 (Figure 3A); i.e., phosphate binds to the enzyme and the enzyme−substrate (ES) complex with a same inhibition constant, wherein the enzyme−substrate−inhibitor (ESI) ternary complex is inactive, while F⁻ was found to be an *uncompetitive inhibitor* toward peptide hydrolysis (*54, 55*). Similar inhibition patterns should be observed for BNPP hydrolysis by *Sg*AP if BNPP is recognized and hydrolyzed in a similar fashion as peptide substrates. On the contrary, phosphate is a *competitive inhibitor* toward BNPP hydrolysis, with K_i ranging from 2.31 to 315 mM at pH 5.0−9.0 (Figure 3B and Table 2), whereas F⁻ is *not an inhibitor* toward BNPP hydrolysis but is a weak activator, which decreases the K_m value with a dissociation constant of 238 mM at pH 8.0 (Figure 3C and Table 2). Similar to F⁻, Cl⁻ and I⁻ are also very weak activators toward BNPP hydrolysis, exhibiting large dissociation constants estimated to be 1.6 and 11 M. For a comparison, K_i values for phosphate and fluoride toward Leu-*p*NA hydrolysis are 30 and 21 mM, respectively, at pH 8.0 (*55*).
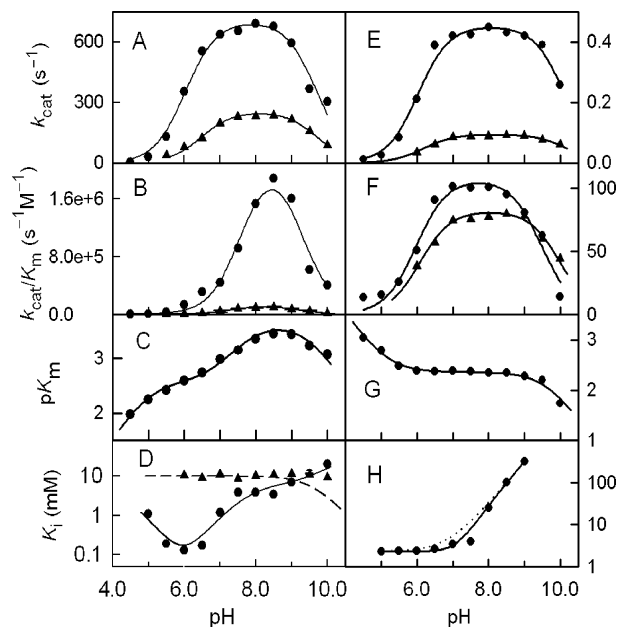
Table 3: pH Dependence of k_{cat} and k_{cat}/K_m for Hydrolyses of Amino Acid-*p*NA and BNPP[a]

		Leu-*p*NA	Met-*p*NA	Lys-*p*NA	BNPP
k_{cat}	pK_{es1}	6.00 ± 0.03 (6.47 ± 0.07)[b]	5.86 ± 0.03	5.7 ± 0.1	6.10 ± 0.04 (6.17 ± 0.08)
	pK_{es2}	9.3 ± 0.3 (9.7 ± 0.7)	9.9 ± 0.5	10.3 ± 0.3	9.6 ± 0.3 (10.2 ± 0.5)
k_{cat}/K_m	pK_{e1}	7.41 ± 0.05 (7.3 ± 0.2)	7.25 ± 0.09	7.0 ± 0.1	5.58 ± 0.04 (6.08 ± 0.07)
	pK_{e2}	9.0 ± 0.4 (9.1 ± 0.7)	9.1 ± 0.5	10.7 ± 0.4	9.29 ± 0.4 (10.0 ± 0.7)

[a] The pH profile of K_m reveals the pK_a values 5.2, 6.5, 7.5, and 9.4 in Leu-*p*NA hydrolysis, 5.2 and 9.6 in BNPP hydrolysis (Figure 4), and 5.5, 6.4, 7.8, and 9.1 from the pK_i−pH profile of ABP toward Leu-*p*NA hydrolysis. [b] pK_a values for the phenylglyoxal-modified enzyme are in parentheses.

The different inhibition patterns toward peptides and BNPP hydrolyses by *Sg*AP offer an opportunity to reveal mechanistic differences between these two substrates.

pH Dependence of Peptide Hydrolysis. The hydrolysis of Leu-*p*NA by *Sg*AP shows a bell-shaped activity−pH profile between pH 4.5 and 10.0 (Figure 4). Nonlinear regression fitting of the k_{cat}−pH profile with a double-deprotonation process (eq 1) gives two ionization constants pK_{es1} = 6.00 and pK_{es2} = 9.3 in the ES complex (Figure 4A and Table 3). The pK_{es1} value is close to that of a metal-bound water in hydrolytic metalloenzymes, such as 6.0−6.2 in carboxypeptidase A toward different substrates (*74*) and 5.0 in thermolysin (*75*). No other residue near the active site of *Sg*AP (*42−44*) can have a pK_a of 6.00. By default, a coordinated water is the best candidate to afford this pK_a

value. The nucleophilic water molecule is likely to be bound to only one metal ion, such as in the case of carboxypeptidase A and thermolysin, because the acidity of a bridging water molecule is influenced by two Lewis acidic metal centers and thus is expected to have a much lower pK_a value.

The pH profile of k_{cat}/K_m of Leu-pNA hydrolysis by SgAP shows two ionization processes with $pK_{e1} = 7.41$ and $pK_{e2} = 9.0$ (Figure 4B and Table 3), attributable to two catalytically important ionizable groups in the free enzyme and/or substrate (62, 63). The pK_{e1} value is close to the pK_a value of the amino group of Leu-pNA (7.94 or 7.74) (76) and is much higher than pK_{es1} in the k_{cat}–pH profile. This pK_{e1} value is probably due to the amino group, which may be required at the TS‡ during SgAP catalysis, as suggested in the crystal structures of inhibitor-bound blAP (48, 49, 56–58). However, the small difference between the pK_{e1} value and the intrinsic pK_a of Leu-pNA reflects a weak affinity for the binding of the deprotonated amino group of Leu-pNA to the enzyme (i.e., $10^{-7.41}/10^{-7.94} = 3.4$ M^{-1}). In ApAP, pK_{e1} was determined to be 7.55 (76), also suggesting a weak binding of the deprotonated amino group.

The second ionization in the pH profiles of k_{cat} and k_{cat}/K_m is similar, which can be attributed to a general acid involved in the binding of the substrate and stabilization of the TS‡. A van't Hoff plot of pK_a (from activity–pH profiles) versus $1/T$ affords the heat of ionization ΔH_{ion} values of 36 ± 3 and 29 ± 2 kJ/mol for pK_{es1} and pK_{es2}, respectively (Figure 2B). These values are comparable to those of histidyl imidazole of ~30 kJ/mol, Tyr of ~25 kJ/mol, and coordinated water of ~25–35 kJ/mol but too large for a carboxylic acid (~3 kJ/mol) and too small for an amine (~50 kJ/mol) or a guanidine (52 kJ/mol) group (77, 78). The presence of an ionizable His can be eliminated because there is no His, other than the metal-bound His residues, near the active site (42–44). The ΔH_{ion} value of pK_{es2} is consistent with that of a tyrosine, e.g., Tyr246 within hydrogen-bonding distance of the "bound phosphate" (42–44). This tyrosine is one major difference in the active sites between SgAP and ApAP, which is aligned with Ile255 in ApAP. The lack of a pK_a value at pH 9–11 in ApAP (76) suggests that Tyr246 is a general acid in SgAP. A recent mutation study on Tyr246 showed a ~100-fold decrease in k_{cat} upon mutations, which also indicated its involvement in SgAP catalysis (79).

The ionization constants revealed in the pH profile of pK_m are in general agreement with those obtained from the pH profiles of k_{cat} and k_{cat}/K_m, except the one at 5.20 (Figure 4C and Table 3). This ionization may be attributed to an acidic residue involved in SgAP catalysis, such as Glu131 close to the active-site metal ions [$M_{1/2}$–O$_{\epsilon1/\epsilon2}$ = 4.21 and 4.42 Å in the Protein Data Bank (PDB) structure 1XJO], and is within hydrogen-bonding distance of the substrate (42, 44). Recent mutagenesis studies of SgAP and ApAP revealed that Glu131 (Glu151 in ApAP) is indeed catalytically significant (79, 80).

Two pK_{es} values of 5.86 and 9.9 were revealed in the k_{cat}–pH profile for Met-pNA hydrolysis, and two pK_e values of 7.25 and 9.1 were revealed in the k_{cat}/K_m–pH profile. Likewise, two pK_{es} values of 5.7 and 10.3 and two pK_e values of 7.0 and 10.7 were revealed in Lys-pNA hydrolysis (Table 3 and Figure 5). Consistent with the low affinity for the binding of the amino group to the metal center in Leu-pNA hydrolysis is the small difference between the pK_{es1} values
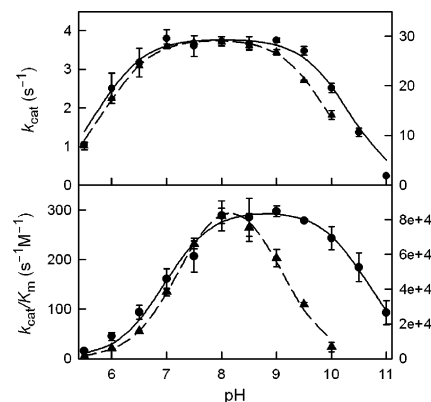

FIGURE 5: pH influence toward the hydrolysis of Lys-pNA (●, left scale) and Met-pNA (▲, right scale) by SgAP.

in hydrolyses of Met- and Lys-pNA, and their intrinsic pK_a values were determined to be 6.95 and 6.83, respectively. The similar pK_{e2} values of the substrates (except Lys-pNA) reflect the involvement of a same general acid in their hydrolyses, suggested to be Tyr246 discussed above. The significantly different pK_{e2} value in Lys-pNA hydrolysis may be attributed to the involvement of the positively charged side-chain amino group ($pK_a = 10.0$) in the hydrolysis, which needs future verification.

Product Inhibition in Peptide Hydrolysis. The crystal structures of amino-acid-bound SgAP (Leu, Phe, or Met) (43, 44) indicate that a stable enzyme–product complex can be expected before the release of the amino acid product. Leu inhibition toward the hydrolysis of Leu-pNA at pH 8.0 shows a competitive inhibition pattern ($K_i = 10.3$ mM), consistent with the involvement of a weak enzyme–product complex during the action of this enzyme. The K_i value of Leu has been determined in the range of pH 6–10 to provide a clearer picture about product binding (▲ in Figure 4D). The pK_a values of the carboxylic and amino termini in Leu are 2.4 and 9.6, respectively (- - - in Figure 4D). However, there is no ionizable group identified in the pK_i–pH plot that can influence product binding to the enzyme at pH 6–10. This result indicates that the ionization of the amino terminus of the Leu product is not significant for its binding with the enzyme prior to its release. Binding of the amino group of Leu to the metal is expected to lower the pK_a of the amino group to less than 9.6, which is not observed. Conversely, the pH dependence of ABP inhibition shows four ionization constants (● in Figure 4D and Table 3).

BNPP Hydrolysis and Inhibition. The hydrolysis of BNPP by SgAP shows a normal bell-shaped activity–pH profile between pH 4.5 and 10.0. The k_{cat}–pH profile reveals two ionization constant pK_{es} values of 6.10 and 9.6 (Figure 4E and Table 3). These values are similar to those in the k_{cat}–pH profile for Leu-pNA hydrolysis and thus are probably attributed to the same ionizable groups, i.e., a coordinated water and Tyr246, respectively. The first pK values in the pH profiles of k_{cat} and k_{cat}/K_m differ by 0.5 units in BNPP hydrolysis but 1.5 units in peptide hydrolysis (Table 3). Because BNPP has no ionizable group at pH 4.5–10.0, the first ionization constants are thus expected to be similar and assigned to the ionization of the nucleophilic water, whereas they are different in Leu-pNA hydrolysis, attributed to the amino group of the substrate as described above. Similar to the case for peptide hydrolysis, the K_m–pH profile for BNPP

hydrolysis (Figure 4G) reveals a pK_a of 5.15. This observation indicates that an acidic group in the active site of *Sg*AP, such as Glu131, is involved in substrate binding and/or catalysis.

The pK_i–pH profile of phosphate toward BNPP hydrolysis (Figures 3B and 4H) cannot be well-fitted to a single-ionization process (··· in Figure 4H) yet can be fitted to a two-ionization process with pK_a values of 7.6 and 11.5 (— in Figure 4H) possibly because of phosphate ionization. The sharp increase in the K_i value after the second ionization suggests that both mono- and dibasic phosphates are stronger inhibitors than the fully deprotonated phosphate toward BNPP hydrolysis by *Sg*AP.

pH Dependence of Modified SgAP. The pH profiles of phenylglyoxal-modified *Sg*AP toward Leu-*p*NA hydrolysis (▲ in parts A and B of Figure 4 and Table 3) show that the pK_{es} values have a larger change than the pK_e values (0.45 versus 0.13 units on average), reflecting that Arg modification influences the ES complex more than free enzyme and that an Arg may be involved in stabilizing the TS‡. The maximum k_{cat} at pH 8.0 decreases by 65%, and k_{cat}/K_m decreases significantly by 95% (partially because of the increase in K_m) relative to the native enzyme upon the modification. The decreases can be attributed to a change of ~2–6 kJ/mol in the activation energy at 298 K, which can be easily achieved by a slight change in interaction at the TS‡ associated with the modification. Because $K_m = k_{cat}/k_1 + k_{-1}/k_1$, a significant decrease in k_{cat} and increase in K_m reflects a significant increase in the dissociation constant k_{-1}/k_1 of the ES complex in the modified enzyme.

The pH profiles of phenylglyoxal-modified *Sg*AP toward BNPP hydrolysis (▲ in parts E and F of Figure 4 and Table 3) show that the pK_e values have a larger change than the pK_{es} values (0.65 versus 0.34 units on average), indicating that Arg modification has a more significant influence on the free enzyme than the ES complex, as opposed to peptide hydrolysis. The k_{cat} at pH 8.0 decreases by 80% (attributed to a small change of 0.6 kJ/mol in the activation energy at 298 K), and the k_{cat}/K_m decreases by only 22% relative to the native enzyme upon the modification, which is likely due to a small change in interaction at the TS‡ associated with an Arg side chain.

Proton Inventory and Viscosity Dependence. Proton inventory was utilized to reveal subtle mechanistic differences between peptide and BNPP hydrolyses by *Sg*AP (*65*). Plots of rate constants with respect to the deuterium atom fraction *n* are shown in Figure 6. The proton inventory of k_{cat} for Leu-*p*NA hydrolysis is not linear, which can be fitted to eq 5 (● in Figure 6A), suggesting a multi-proton-transfer process at the TS‡ in peptide hydrolysis. Conversely, BNPP hydrolysis has a linear correlation (with a correlation coefficient of 99.9%, ● in Figure 6B), indicating a single-proton-transfer process at the TS‡ during its hydrolysis by *Sg*AP.

Proton inventory of k_{cat}/K_m for Leu-*p*NA hydrolysis is linear with a small isotope effect (○ in Figure 6A), attributed to a similar pattern and magnitude in the change of k_{cat} and K_m with respect to *n*. Because $K_m = k_{-1}/k_1 + (1/k_1)k_{cat}$, the similar change in magnitude of K_m and k_{cat} with respect to *n* suggests that the dissociation constant of the ES complex k_{-1}/k_1 may not have a significant change with *n*. This observation reflects that hydrogen bonding may not be
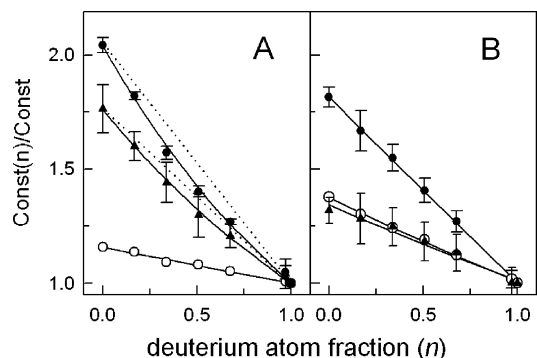

FIGURE 6: Proton inventory of k_{cat} (●), K_m (▲), and k_{cat}/K_m (○) for the hydrolyses of (A) Leu-*p*NA and (B) BNPP by *Sg*AP at pH/pD 8.0. The solid lines/curves are the best fits, and the dotted lines in A represent a linear one-proton-transfer process.

involved in the binding of peptide substrates with *Sg*AP. Conversely, the K_m value of BNPP hydrolysis (▲ in Figure 6B) shows a smaller isotope effect, which results in a more significant isotope effect on k_{cat}/K_m than that in Leu-*p*NA hydrolysis (○ in Figure 6B). A larger decrease in k_{cat} than K_m with increasing amounts of D$_2$O suggests a possible increase in k_{-1} and/or decrease in k_1, which results in a decrease in k_{-1}/k_1 for BNPP binding to the enzyme. This result suggests the involvement of hydrogen bonding for the binding of BNPP to the enzyme, which is disturbed upon deuteration.

*Sg*AP exhibits a large k_{cat}/K_M of ~10^6 M^{-1} s^{-1} toward Leu-*p*NA hydrolysis, suggesting that the reaction may be partially diffusion-controlled as observed in chymotrypsin catalysis (*67*). In the latter case, the hydrolyses of the fast substrates *N*-(methoxycarbonyl)-L-tryptophan *p*-nitrophenyl ester (3.5 × 10^7 M^{-1} s^{-1}) and *N*-acetyl-L-tryptophan methyl ester (8 × 10^5 M^{-1} s^{-1}) show significant diffusion-limited contribution to the reaction rate, whereas hydrolysis of the slow substrate *N*-acetyl-L-tryptophan *p*NA (300 M^{-1} s^{-1}) does not. Because the viscosity of D$_2$O at 25 °C is 23% higher than that of H$_2$O (*81*), it is also important to reveal whether or not the reaction rate is affected by viscosity in the proton inventory studies. The results show that the increase in viscosity of the solution (in the form of the relative viscosity of the solution in the presence and absence of the viscosogenic agent sucrose, $n_{rel} = \eta/\eta_o$, eqs 6 and 7) does not decrease the rate constants of Leu-*p*NA and BNPP hydrolysis by *Sg*AP (Figure 7).

BNPP Hydrolysis by ApAP and Phosphate Inhibition. BNPP hydrolysis by an analogous dinuclear AP was investigated to determine whether or not the unexpected catalytic promiscuity is unique to *Sg*AP. *Ap*AP shares with *Sg*AP 29.6% sequence homology, a similar tertiary folding pattern (<1.8 Å deviation for 70% of the α carbons), and a virtually identical active-site coordination sphere (*42–47*). Despite the similarity, the hydrolysis of 3.0 mM BNPP by 14.5 nM *Ap*AP monitored for 28 h revealed a 300 times slower hydrolytic rate of 1.69 × 10^{-8} mM/s than that by *Sg*AP under the same conditions. Nevertheless, this rate is still much greater than the nonenzymatic hydrolytic rate, indicating the significance of dinuclear centers in hydrolytic enzyme catalyses. The 300-fold slower rate is equivalent to an increase in E_a by 14 kJ/mol at 25 °C, which suggests a possible involvement of a hydrogen-bonding/electrostatic interaction to assist BNPP hydrolysis by *Sg*AP. BNPP was
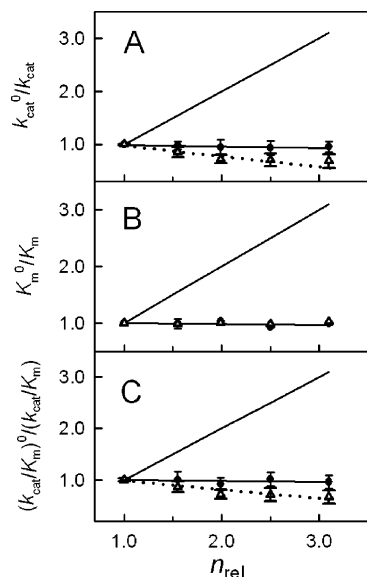
FIGURE 7: Influence of solvent viscosity toward the hydrolysis of Leu-pNA (●) and BNPP (△) in terms of k_{cat} (A), K_m (B), and k_{cat}/K_m (C) in the presence of 0, 16, 23, 30, and 35% (w/v) sugar in 20 mM HEPES at pH 8.0 containing 10 μM Zn^{2+}, 0.10 M NaCl, and 10 mM CaCl$_2$. The theoretical influence of viscosity on a fully diffusion-controlled reaction is presented as the solid line with a slope of 1.
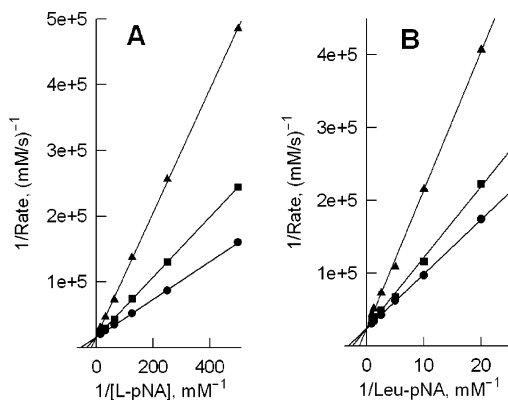

FIGURE 8: (A) BNPP (2.0 and 12 mM) inhibition toward hydrolysis of Leu-pNA by ApAP in 0.10 M HEPES at pH 8.0. (B) Phosphate (100 and 400 mM) inhibition toward the hydrolysis of Leu-pNA by ApAP in 0.10 M MES at pH 6.0. Competitive inhibition patterns are observed in both cases.

found to be a competitive inhibitor toward Leu-pNA hydrolysis by ApAP at pH 8.0 with K_i = 8.1 mM (Figure 8A), which reflects that BNPP may compete with peptide binding in ApAP. Phosphate was previously determined to be a strong *noncompetitive* inhibitor toward Leu-pNA hydrolysis by SgAP, whereas it has been determined herein as *not an inhibitor* at pH 8.0 and a very weak *competitive* inhibitor at pH 6.0 toward Leu-pNA hydrolysis by ApAP (Figure 8B and Table 2). However, fluoride was found to exhibit the same *uncompetitive* inhibition pattern toward peptide hydrolysis by these two enzymes (*55, 82*).

DISCUSSION

Catalytic Promiscuity of SgAP toward BNPP Hydrolysis. The structure of phosphoesters resembles the tetrahedral *gem-*diolate-like TS‡ of the peptide during hydrolysis, which explains why BNPP and NPP are inhibitors toward SgAP and ApAP (Table 2). Moreover, BNPP and a few phospho-

esters and fluorophosphates are also known to serve as suicide substrates against serine proteases and esterases, such as trypsin, chymotrypsin, and acetylcholine-esterase (*5–7*). In this case, the nucleophilic serine in the active site attacks the phosphocenter to form the covalent phosphoester linkage Ser$-$O$-$P(O)$_2$$^-$$-$OR with concomitant cleavage of a phosphoester or the P$-$F bond, resembling the "initial burst" kinetics of serine proteases toward peptide hydrolysis. However, the TS‡-mimicking phospho-serine moiety here is indefinitely stable with respect to the time scale of the catalytic rates of these enzymes. On the other hand, similar to the cleavage of the phosphodiester BNPP by SgAP (*20, 21*), the recently demonstrated sulfinamide bond cleavage by subtilisin is also a novel observation of catalytic promiscuity in the serine protease family (*83*).

Owing to the very different nature of peptides and phosphoesters, a direct comparison of the rates of their hydroyses by SgAP has little meaning. Nevertheless, the rate constants for BNPP hydrolysis are comparable to those of the less specific peptide substrates (Table 2). Moreover, the catalytic efficiency of 124 M^{-1} s^{-1} for BNPP hydrolysis by SgAP is much higher than or comparable to those by some natural phosphoester-hydrolyzing enzymes and their derivatives, such as BNPP hydrolysis by alkaline phosphatase (0.05 M^{-1} s^{-1}) (*84*) and *Burkholderia* phosphonate monoester hydrolase (11.4 M^{-1} s^{-1}) (*85*) and ethyl(p-nitrophenyl)-phosphate hydrolysis by metal derivatives of *Pseudomonas* phosphotriesterase (1.1$-$7.2 M^{-1} s^{-1}) (*86*). The rate constants are also dramatically greater than those of many synthetic chemical model systems of Zn^{2+} complexes (e.g., in the range of $k_2 \sim 10^{-6}$ to 10^{-4} M^{-1} s^{-1}) at >35 °C and pH > 8.5 (*25–31*). The specific activity toward the hydrolysis of 1.0 mM BNPP (190 nmol min^{-1} mg^{-1}, derived from the Michaelis$-$Menten equation) is also in the range of those of several phosphodiesterases and phosphatases (0.3$-$2450 and $\sim$2$-$40 nmol min^{-1} mg^{-1}, respectively) (*87, 88*). Nevertheless, a native phosphodiester-specific enzyme can show a much higher activity, such as the phosphodiesterase gene product of *ElaC*, which shows a k_{cat} of 59 s^{-1} and k_{cat}/K_m = 14 750 M^{-1} s^{-1} (*89*). Because SgAP is known to be an aminopeptidase on the basis of its primary and tertiary structures with a high specificity toward a hydrophobic N terminus, its activity toward the hydrolysis of a phosphodiester bond can be considered a novel phenomenon.

BNPP hydrolysis by SgAP has a K_m value 5 times greater and a k_{cat} value more than 1000-fold less than the corresponding values for the specific peptide substrate Leu-pNA (Table 1), indicating that BNPP hydrolysis would have a much larger dissociation constant (k_{-1}/k_1) for its ES complex than Leu-pNA. This is also the case when compared to those less specific peptide substrates. These comparisons suggest that BNPP is not recognized as a true TS‡ analogue as α-aminophosphonates and bestatin with submicromolar inhibition constants (Table 2), which may be attributed to the lack of the α-amino group and a less specific hydrophobic moiety.

In addition to BNPP, the phosphonate ester p-nitrophenyl phenylphosphonate was previously found to be hydrolyzed by SgAP, with k_{cat} = 0.014 s^{-1} and k_{cat}/K_m = 0.94 M^{-1} s^{-1} (*21*), which is nevertheless still much higher than that by alkaline phosphatase (0.030 M^{-1} s^{-1}) (*84*). However, the phosphomonoester NPP is not hydrolyzed by SgAP under

the same conditions but by an inhibitor (Table 1). These results indicate that the catalytic promiscuity of *Sg*AP exhibits catalytic specificity, characteristic of enzyme catalysis.

Catalytic Proficiencies of SgAP. The catalytic proficiencies (*90*) for Leu-*p*NA hydrolysis by *Sg*AP at pH 8.0 are 6.7 × 10^9 and 8.2 × 10^{14}, respectively, in terms of the first-order rate constants (*91*) k_{cat}/k_o and the catalytic efficiency (*92*) $(k_{cat}/K_m)/k_w$ with respect to the rate constants k_o and $k_w = k_o/[H_2O]$ for nonenzymatic hydrolysis under the same conditions (footnote c in Table 1). The k_{cat}/k_o value of 6.7 × 10^9 for Leu-*p*NA hydrolysis represents a dramatic $\Delta(\Delta G^\ddagger)$ value of −57 kJ/mol at 303 K with respect to the uncatalyzed reaction. The catalytic proficiencies are much smaller for the less specific peptide substrates (Table 1).

Despite the presence of the good leaving group *p*-nitrophenol, the nonenzymatic hydrolytic rate of BNPP is still *extremely slow*, with a rate constant $k_o = 1.1 \times 10^{-11}$ s^{-1} at pH 7.0 and 25 °C (*93*), 3.0 × 10^{-10} s^{-1} at pH 7.0 and 50 °C (*94*), or 6.3 × 10^{-8} s^{-1} at pH 10.0 and 100 °C (*95*), which is equivalent to a large $\Delta G^\ddagger$ value of 138 kJ/mol and a half-life of ~2000 years. The pH range for maximum catalysis of BNPP hydrolysis by *Sg*AP is around 7.0−9.0 (Figure 4). Thus, enormous catalytic proficiencies of $k_{cat}/k_o = 3.85 \times 10^{10}$ and $(k_{cat}/K_m)/k_w = 5.1 \times 10^{14}$ and a half-life of ~2 s are obtained for BNPP hydrolysis by *Sg*AP around neutral pH. The k_{cat}/k_o ratio represents a $\Delta(\Delta G^\ddagger)$ value of −62 kJ/mol at 303 K, relative to uncatalyzed hydrolysis. This magnitude is greater than that for Leu-*p*NA hydrolysis, which indicates that the stabilization of the TS‡ complex in BNPP hydrolysis by *Sg*AP is equally efficient as in peptide hydrolysis.

This nearly 4 × 10^{10}-fold enhancement of BNPP hydrolysis by *Sg*AP is quite remarkable because phosphoesters are not supposed to be effectively hydrolyzed by peptidases, owing to their significantly different structures from those of peptides and the analogy between phosphoesters and the *gem*-diolate-like TS‡ of peptides during hydrolysis. The $\Delta G^\ddagger$ value is usually larger for the hydrolysis of phosphoester bonds than peptide bonds (e.g., 64 and 41 kJ/mol based on k_o for uncatalyzed hydrolyses of BNPP and Leu-*p*NA at 303 K, respectively). Moreover, the negatively charged phospho-moiety in phosphodiesters is unfavorable for nucleophilic attack by a water molecule (in the form of hydroxide) because of electrostatic repulsion, which results in the slow rate of uncatalyzed hydrolysis of phosphodiester (*96*, *97*). The proficient hydrolysis of the phosphodiester by *Sg*AP thus represents a very unique case of enzyme catalytic promiscuity.

Alkaline phosphatase has recently been revealed to exhibit a catalytic promiscuity, wherein arylsulfate and BNPP are hydrolyzed with k_{cat}/K_m values of 0.01 and 0.05 M^{-1} s^{-1} and a rate enhancement of ~10^9 for the former relative to the uncatalyzed reaction (*84*, *92*). The similar structures and TS‡ configurations of the native phosphomonoester substrates and the alternative substrates arylsulfate and BNPP and the structural homology between alkaline phosphatase and aryl sulfatase (*98*−*100*) may in part account for the catalytic promiscuity. Conversely, the case discussed herein for the proficient BNPP hydrolysis by *Sg*AP is quite unique because the structures of peptides and phosphodiesters and their TS‡ configurations are very different. Besides, there is no

sequence and structural homology between *Sg*AP and phosphoester-hydrolyzing enzymes.

Thermodynamics of the Hydrolyses of Peptides and BNPP. The configurations of a specific substrate and the corresponding enzyme molecule are properly oriented in the ES complex and thus do not require much loss in the degree of freedom for the subsequent formation of the TS‡ complex, which results in a smaller $-\Delta S^\ddagger$ value, whereas it is just the opposite for less specific substrates. Indeed, larger $-\Delta S^\ddagger$ values were found in the hydrolysis of less specific substrates by chymotrypsin (*101*, *102*), which has been explained by the requirement of "freezing" the substrates to a larger extent at the TS‡ to orient the substrates for nucleophilic attack.

The much larger $-\Delta S^\ddagger$ value for BNPP hydrolysis than Leu-*p*NA hydrolysis by *Sg*AP (Table 1) indicates a significant loss in the degree of freedom at the TS‡ in BNPP hydrolysis, which maybe partially attributable to the loss in the degree of freedom because of salvation. Nevertheless, the value is close to that for the hydrolysis of dimethylphosphate by nucleophilic anions ($\Delta S^\ddagger = -143$ J K^{-1} mol^{-1}) (*103*) and basic hydrolysis of BNPP (−107 J K^{-1} mol^{-1}) at pH 7.0 and 50 °C (*94*) and at pH 8.0 and 30 °C (Table 1). These observations reflect a lack of significant pre-reorientation upon BNPP binding to *Sg*AP. Phosphoester hydrolysis follows an "in-line" S$_N$2 inversion pathway (*13*, *14*), wherein the phosphoesters are oriented in such a way so that the attacking nucleophile and the leaving group are aligned at the axial positions in the trigonal bipyramidal TS‡. This structural restriction may cause a significant loss in the degree of freedom at the TS‡, resulting in a large $-\Delta S^\ddagger$ value in phosphoester hydrolysis.

The hydrolyses of BNPP and peptides by *Sg*AP exhibits similar $\Delta H^\ddagger$ values (Table 1), suggesting that they are likely to involve similar interactions in hydrolysis. Conversely, $\Delta H^\ddagger$ in BNPP hydrolysis by *Sg*AP is smaller than nonenzymatic hydrolysis of phosphodiesters, e.g., 74 kJ/mol smaller than that of $(CH_3O)_2OPO_2^{2-}$ (*103*), 52.6 kJ/mol smaller than that of BNPP (Table 1), and ~20−50 kJ/mol smaller than that of BNPP hydrolysis by several metal complexes (*104*). The decrease may be attributable to hydrogen bonding (~15−30 kJ/mol for each hydrogen bond), coordinating to the metal, and/or other interactions, which can stabilize the TS‡ by *Sg*AP.

Peptide versus BNPP Hydrolysis by SgAP. On the basis of the similar pH−k_{cat} profiles in peptide and BNPP hydrolyses (Figure 4), the ionizable groups involved in both hydrolyses are probably the same. The similar $\Delta H^\ddagger$ values in peptide and BNPP hydrolyses reflect that similar interactions might be involved at the rate-determining step in both hydrolyses. However, the different results in the proton inventory studies indicate a difference at the rate-determining steps in these two catalyses. The difference is presumably due to the fact that the peptidyl −(CO)−NH− bond is hydrolyzed to produce the zwitterion form of Leu (containing COO$^-$ and NH$_3^+$) and the neutral *p*NA, while the phosphodiester bond (Ar−O)$_2$−PO$_2^{1-}$ is hydrolyzed to give a phosphomonoester (ArO−PO$_3^{2-}$) and *p*-nitrophenol. Peptide hydrolysis thus involves at least a two-proton transfer at the rate-determining step, while BNPP hydrolysis involves one proton.

Despite the same inhibition pattern and similar inhibition constants for most inhibitors toward the hydrolyses of

peptides and BNPP by *Sg*AP (Table 2), F⁻ and phosphate show different inhibition patterns toward these two substrates, which suggest mechanistic differences between these two hydrolytic reactions. The uncompetitive inhibition pattern of F⁻ toward peptide hydrolysis (*55*) suggests that the nucleophilic water becomes available for F⁻ substitution only after the binding of the peptide substrate, whereas the noninhibitory nature of F⁻ toward BNPP hydrolysis suggests that the nucleophilic coordinated water in BNPP hydrolysis is not replaceable by F⁻ and may not be the same one as that in peptide hydrolysis. The different inhibition constants of F⁻ toward peptide and BNPP hydrolyses (Table 2) are also consistent with the different interactions of F⁻ with the enzyme in these two reactions.

The similar phosphate inhibition constants in the hydrolyses of BNPP and Leu-*p*NA by *Sg*AP (Table 2) reflect similar phosphate binding to the enzyme in these two reactions, while the different inhibition patterns in these two reactions indicate that the two substrates may not bind to *Sg*AP in the same way. Because the bindings of phosphate and peptide to the enzyme are not exclusive (i.e., a noncompetitive inhibition), the phosphate-binding site cannot be the substrate-binding metal center. One candidate can be the side chain of Arg202 close to the active site (Figure 1) because phosphate is known to bind the Arg residue in several enzymes (*105−110*). Our recent ³¹P NMR relaxation study of phosphate binding to CoZn-*Sg*AP indicates that phosphate is at least 4.1 Å away from the metal, precluding direct metal binding (*55*). The positive side chain of Arg202 may stabilize the *gem*-diolate-like TS‡ of a peptide yet not necessarily be involved in the binding of the peptide, which can thus form both the EI and ESI complexes to exhibit noncompetitive inhibition. If Arg202 is involved in BNPP binding, the binding of phosphate to Arg202 may prevent BNPP binding to exhibit a competitive inhibition pattern.

*Ap*AP and *Sg*AP show different rates toward BNPP hydrolysis and different phosphate inhibition patterns toward peptide hydrolysis, suggesting that they bind phospho-moieties differently. However, their similar fluoride inhibition pattern toward peptide hydrolysis (*55, 82*) suggests a similar mechanism for the generation of the nucleophilic water. The competitive phosphate inhibition toward peptide hydrolysis by *Ap*AP (Figure 8B) indicates that phosphate and peptide bindings are exclusive, with the active-site metal center being the most likely candidate for phosphate binding. The weak phosphate inhibition and the low activity toward BNPP hydrolysis by *Ap*AP further suggest that Arg202 may play a key role in *Sg*AP action, because *Ap*AP lacks such an amino acid near the active site. Herein, *Ap*AP serves as a "natural variant" of *Sg*AP and has provided further information about phosphate binding and the catalytic promiscuity of *Sg*AP. The results also indicate that the catalytic promiscuity of *Sg*AP toward phosphodiester bond cleavage is a unique property of this enzyme, which is not shared by analogous peptidases.

The significant difference in the k_{cat}/K_m−pH profiles between BNPP and Leu-*p*NA hydrolyses reflects the involvement of a different ionizable group in the hydrolysis of these two substrates, most likely the amino group of the peptide substrate that is deprotonated and bound to one active-site metal based on crystallographic studies of EI complexes of *Ap*AP and blAP (*45−49*). There is no

ionization for BNPP in the pH range conducted, indicating that BNPP ionization should not affect the rate of hydrolysis by *Sg*AP under the experimental conditions.

In Leu-*p*NA hydrolysis, a decrease in K_m and an increase in k_{cat} with an increasing pH in the acidic region (Figure 4) reflects a decrease in k_{-1} and/or an increase in k_1, which results in a smaller dissociation constant (k_{-1}/k_1) of the ES complex, whereas an increase in both K_m and k_{cat} with an increasing pH in BNPP hydrolysis (Figure 4) reflects the fact that the k_{-1}/k_1 value is less influenced by pH. A pK_a of 5.1 is revealed from the K_m−pH profiles of both reactions (parts C and G of Figure 4), likely because of Glu131 (Figure 1). The repulsion between Leu-*p*NA and Glu131 greatly decreases with an increasing pH around pH 7.5 when Glu131 is deprotonated and the amino group of Leu-*p*NA is still protonated. Conversely, the negative BNPP in the pH range of the experiment renders charge repulsion with deprotonated Glu131. The pK_a of 5.5 revealed in the pK_i−pH profile of ABP (Figure 4D and Table 3) also suggests that this ionization can enhance ABP binding to the enzyme.

The catalytic pathways of these two structurally diverse peptide and phosphodiester substrates by *Sg*AP are largely different. In summary, (i) peptides and BNPP bind to the same active site but with different binding modes; (ii) an Arg, a Tyr, and a Glu/Asp are revealed to be important residues in the action of this enzyme; (iii) different water molecules serve as the nucleophiles in the hydrolyses of peptides and BNPP; (iv) the rate-limiting step is different in these two hydrolytic reactions based on proton inventory; (v) BNPP is suggested to bind to this enzyme analogous to the TS‡ of peptide substrates but does not serve as a true TS‡ analogue; and (vi) the amino terminus of a peptide substrate does not bind tightly to the enzyme and thus is not the key determinant for substrate binding as suggested in static crystallographic studies.

Mechanism for Peptide Hydrolysis by SgAP. The pH−activity profiles reveal that the deprotonation of the peptide substrate is essential for hydrolysis, which, however, may not be the main driving force for binding because of its small intrinsic affinity constant. The crystal structures of phosphonate EI complexes of blAP and *Ap*AP (*48, 49*) may reflect the TS‡ structure but not the binding status of the substrate in the ES complex. In these TS‡−analogue complexes of APs, either the bridging or terminal oxygen of the inhibitor should be equivalent to the bridging or terminal nucleophilic water, respectively, which attacks the peptidyl carbonyl carbon to yield the TS‡. Herein, a deprotonated dipeptide substrate Leu-Phe is superimposed onto the inhibitor in the EI complex, with the amino group bound to the metal close to the hydrophobic recognition site involving Phe219. Then, either the bridging water (mechanism I) or a terminal water (mechanism II) performs nucleophilic attack on the scissile bond.

In mechanism I, Zn1 near the hydrophobic site serves as the binding site for the amino group, whereas Zn2 is off the −HN−CO−C$_\alpha$− plane of the substrate by ∼55°, which would not have feasible orbital overlap with the sp² lone pair of the carbonyl oxygen, and Zn1 is too far away (3.7 Å) to form a bond with the scissile carbonyl. Without the carbonyl group being bound to the metal center for further polarization of the C=O bond, it may not be the preferred mechanistic pathway for peptide hydrolysis by *Sg*AP.
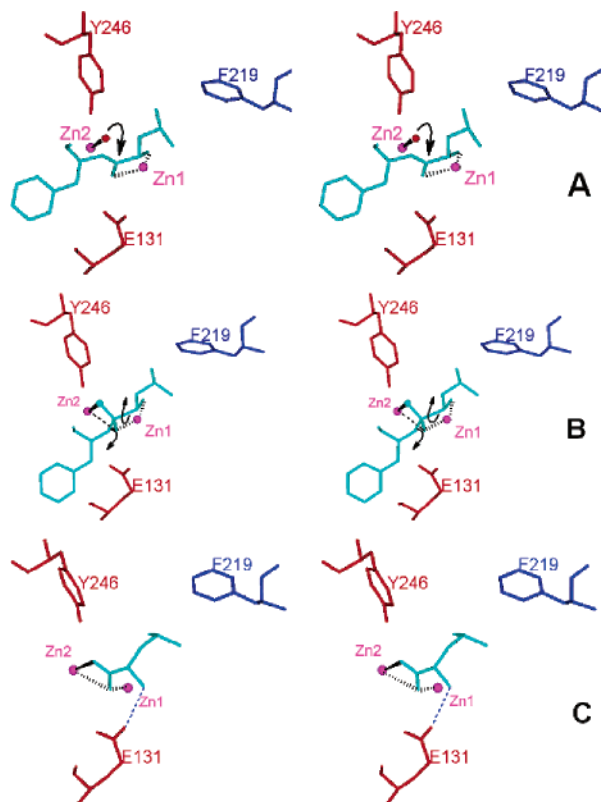
FIGURE 9: (A) Dipeptide Leu-Phe (cyan) is superimposed onto a bound 1-aminophosphonate inhibitor, in which the amino group is bound to Zn1 similar to inhibitor binding and the nucleophilic water is the Zn2-bound terminal water that is hydrogen-bonded to Tyr246 (red sphere). (B) *gem*-diolate-like TS‡ is formed upon nucleophilic attack, followed by breakage of the peptide bond, detachment of the amino group, and rotation of the C$_{\alpha}$−CO bond to afford (C) the Leu-bound structure (PDB 1F2O).

In mechanism II (Figure 9A), both the carbonyl and the deprotonated N-terminal amino groups of the substrate (cyan) are bound to Zn1 near the hydrophobic recognition site to afford a favorable chelating five-member ring M−N−C$_{\alpha}$−C=O. Zn2 is off the peptidyl −HN−CO−C$_{\alpha}$− plane by ∼65° and is thus not expected to bind to the carbonyl oxygen through the sp^2 lone-pair electrons, whereas its coordinated terminal water (red sphere) above the carbonyl acquires a high nucleophilicity via hydrogen bonding with Tyr246. After nucleophilic attack, the carbonyl oxygen adopts sp^3 hybridization and becomes a bridging ligand (Figure 9B). The pK_a of 6.03 for the nucleophilic water and the uncompetitive F$^-$ inhibition (*55*) also agree with this mechanism.

Upon cleavage of the peptide bond, the pK_a of the amino group of the amino acid product increases, which results in the detachment of the amino group from the metal. This is followed by the rotation of the OC−C$_{\alpha}$ bond to adopt the configuration of the bound amino acid (*43, 44*) (parts B and C of Figure 9), wherein the protonated amino group is hydrogen-bonded with Glu131. Releasing the N-terminal amino acid product and binding another substrate start another catalytic cycle.

Mechanism for BNPP Hydrolysis by SgAP. There are two possible mechanisms for BNPP hydrolysis by *Sg*AP (Figure 10): (III) following the same mechanism as peptide substrates (Figure 9B) with a terminal nucleophilic water (Figure
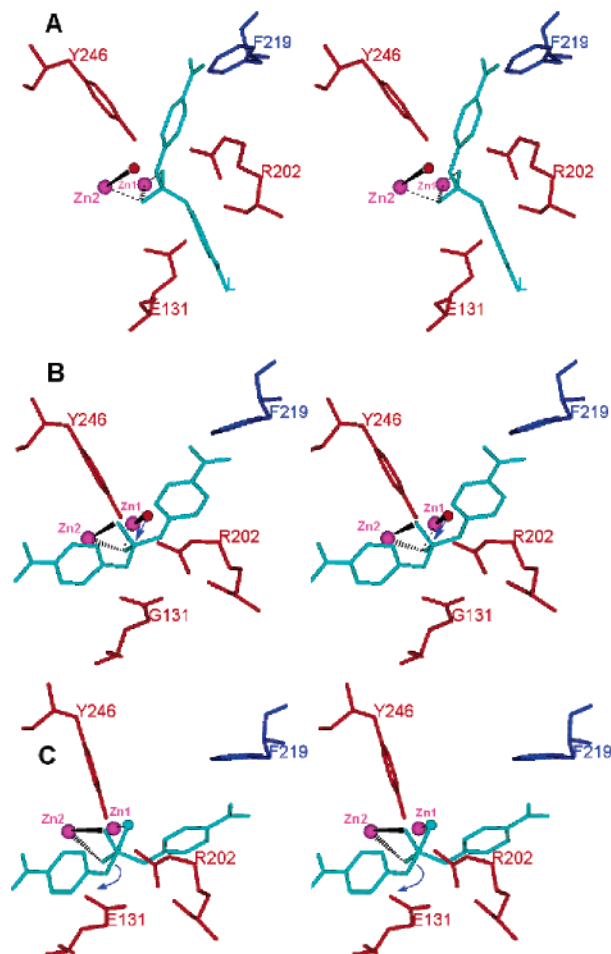

FIGURE 10: (A) BNPP (cyan) is modeled into the active site of *Sg*AP with a binding mode analogous to peptide binding (cf. Figure 9A) and (B) the plausible *gem*-diolate-like TS‡ in peptide hydrolysis (cf. Figure 9B). The nucleophilic water (red sphere) in B is at the "in-line" position trans to the leaving group, whereas this is not the case in A. (D) plausible trigonal bipyramidal TS‡ of the binding model from B.

10A) or (IV) mimicking the binding pattern of the tetrahedral *gem*-diolate-like TS‡ of peptide substrates (Figure 10B).

In mechanism III, BNPP binds to the active-site metal ions via the >PO$_2^-$ moiety, with one oxygen mimicking the amino group and the other oxygen as a bridging ligand (cyan, Figure 10A), resembling the proposed binding mode for peptide substrates (cf. Figure 9A). Herein, the nucleophilic water is the same one as in peptide hydrolysis (red sphere). However, the different phosphate and fluoride inhibition patterns and different proton inventory toward peptide and BNPP hydrolyses reflect that the mechanisms for hydrolyses of these two substrates are different. Moreover, the nucleophilic water is off by ∼35° from the *anti* position with respect to the leaving group (L in Figure 10A), which also encounters steric hindrance with the protein around sequence 201−203. The binding mode with the bridging water as the nucleophile can be excluded because of steric hindrance and the lack of in-line attack trans to the leaving group.

In mechanism IV, the binding mode of BNPP resembles the tetrahedral TS‡ of a peptide substrate (or the binding mode of a 1-aminophosphonate inhibitor) without the amino group (Figures 9B and 10B). A coordinated water on Zn1 in place of the amino group of peptide substrates (red sphere,

Figure 10C) is situated trans to the leaving group (L), ideal for in-line attack at the phosphocenter. The nucleophilic water here is thus not the one in peptide hydrolysis, consistent with the different actions of fluoride in peptide and BNPP hydrolyses. Upon nucleophilic attack, a trigonal bipyramidal TS‡ is formed (Figure 10C), which is followed by cleavage of the phosphoester bond to release *p*-nitrophenol first and then the more tightly bound phosphomonoester product NPP (Table 2) and proceeds with the next catalytic cycle. Herein, Arg202 is proposed to be involved in BNPP binding and hydrolysis but not in the binding of the peptide substrate rather than stabilizing the TS‡ during peptide hydrolysis.

CONCLUDING REMARKS

Proteins from the same evolutionary origin with structural and sequence similarities may have evolved to exhibit completely different functions unrelated to each other, such as between α-lactalbumin and lysozyme (*111–114*), alkaline phosphatase and arylsulfatase (*115, 116*), arsenate reductase and protein phosphatase (*117–119*), and several others (*15–19*). Some of these enzymes can carry out "moonlighting catalyses" in the same active site (*15–19*), which demonstrates their evolutionary correlations and structural similarities. However, it would be unexpected for an enzyme to exhibit an effective alternative catalysis that is normally carried out by an evolutionarily and structurally unrelated enzyme. Alternative enzyme catalyses, although in most cases, show much lower rates relative to the normal catalyses, may provide information about how enzymes function that is otherwise not possible to obtain by the use of normal substrates. We describe in this paper that a phosphodiester substrate is hydrolyzed by *Sg*AP with a significant 4×10^{10}-fold rate enhancement relative to the noncatalyzed reaction at neutral pH and room temperature, which is in the range of native phosphoester-hydrolyzing enzymes and higher than the specific peptide substrates by this enzyme. Despite being an alternative catalysis of *Sg*AP, it also exhibits enzyme-characteristic substrate specificity, discriminating against phosphomonoester, phosphotriester, and phosphonate ester.

Dinuclear centers of different metal ions are found in many hydrolytic enzymes, including urease (Ni), nucleases (Zn), arginase (Mn), prolidase (Mn), and aminopeptidase (Zn or Co) (*16*), as well as in a number of Fe-, Mn-, and Cu-containing oxidases and oxygenases (*120*). The dinuclear active-site feature and the catalytic versatility of *Sg*AP and its metal derivatives entitle this enzyme to serve as an ideal "natural dinuclear model system" for further investigation of dinuclear hydrolysis of both peptides and phosphodiesters and possibly other dinuclear catalyses. Indeed, the di-Cu derivative of *Sg*AP has recently been revealed to exhibit a significant catechol oxidase-like activity toward the oxidation of catechol and derivatives (*121*). *Sg*AP seems to be an enzyme at a catalytic crossroad, which may serve as a "living fossil" to provide further insight into the evolution of enzyme catalysis. Future studies of this unique natural dinuclear model system by means of physical methods and molecular biology are expected to lead us to gain a better understanding of dinuclear hydrolyses and other dinuclear catalyses in chemical and biological systems and further knowledge about how this enzyme has evolved to exhibit the mechanistically diverse activities.

REFERENCES

1. Pauling, L. (1948) Chemical achievement and hope for the future, *Am. Sci. 36*, 51–58.
2. Walsh, C. (1979) *Enzymatic Reaction Mechanisms*, Freeman, New York.
3. Lerner, R. A., Benkovic, S. J., and Schultz, P. G. (1991) At the crossroads of chemistry and immunology: Catalytic antibodies, *Science 252*, 659–667.
4. Wentworth, P., and Janda, K. D. (1998) Catalytic antibodies, *Curr. Opin. Chem. Biol. 2*, 138–144.
5. Nishida, K., Ohta, Y., Ito, M., Nagamura, Y., Kitahara, S., Fujii, K., and Ishiguro, I. (1996) Conversion of γ-glutamylcysteinylethyl ester to glutathione in rat hepatocytes, *Biochim. Biophys. Acta. 1313*, 47–53.
6. Preuss, C. V., and Svensson, C. K. (1996) Arylacetamide deacetylase activity toward monoacetyldapsone—Species comparison, factors that influence activity, and comparison with 2-acetylaminofluorene and *p*-nitrophenyl acetate hydrolysis, *Biochem. Pharmacol. 51*, 1661–1668.
7. Luan, L., Sugiyama, T., Takai, S., Usami, Y., Adachi, T., Katagiri, Y., and Hirano, K. (1997) Purification and characterization of pranlukast hydrolase from rat liver microsomes: The hydrolase is identical to carboxylesterase pI 6.2, *Biol. Pharmacol. Bull. 20*, 71–75.
8. Sträter, N., and Lipscomb, W. N. (1995) Transition state analogue L-leucinephosphonic acid bound to bovine lens leucine aminopeptidase: X-ray structure at 1.65 Å resolution in a new crystal form, *Biochemistry 34*, 9200–9210.
9. Lejczak, B., Kafarski, P., and Zygmunt, J. (1989) Inhibition of aminopeptidases by aminophosphonates, *Biochemistry 28*, 3549–3555.
10. Tronrud, D. E., Holden, H. M., and Matthews, B. W. (1986) Structures of 2 thermolysin—inhibitor complexes that differ by a single hydrogen bond, *Eur. J. Biochem. 157*, 261–268.
11. Giannousis, P. P., and Barlett, P. A. (1987) Phosphorus amino acid analogs as inhibitors of leucine aminopeptidase, *J. Med. Chem. 30*, 1603–1609.
12. Christianson, D. W., and Lipscomb, W. N. (1988) Comparison of caboxypeptidase A and thermolysin inhibition by phosphonamidates, *J. Am. Chem. Soc. 110*, 5560–5565.
13. Cleland, W. W., and Hengge, A. C. (1995) Mechanisms of phosphoryl and acyl transferase, *FASEB J. 9*, 1585–1594.
14. Anderson, M. A., Shim, H., Raushel, F. M., and Cleland, W. W. (2001) Hydrolysis of phosphotriesters: Determination of transition states in parallel reactions by heavy-atom isotope effects, *J. Am. Chem. Soc. 123*, 9246–9253.
15. O'Brien, P. J., and Herschlag, D. (1999) Catalytic promiscuity and the evolution of new enzymatic activities, *Chem. Biol. 6*, R91–R105.
16. Copley, S. D. (2003) Enzymes with extra talents: Moonlighting functions and catalytic promiscuity, *Curr. Opin. Chem. Biol. 7*, 265–272.
17. Yarnell, A. (2003) The power of promiscuity, *Chem. Eng. News 8*, 33–35.
18. Bornscheuer U. T., and Kazlauskas R. J. (2004) Catalytic promiscuity in biocatalysis: Using old enzymes to form new bonds and follow new pathways, *Angew. Chem., Int. Ed. 43*, 6032–6040.
19. Kazlauskas, R. J. (2005) Enhancing catalytic promiscuity for biocatalysis, *Curr. Opin. Chem. Biol. 9*, 195–201.
20. Park, H. I., and Ming, L.-J. (1999) A 10^{10} rate enhancement of phosphodiester hydrolysis by a dinuclear aminopeptidase-transition-state analogue as substarates, *Angew. Chem., Int. Ed. Engl. 38*, 2914–2916.
21. Ercan, A., Park, H. I., and Ming, L.-J. (2000) Remarkable enhancement of the hydrolyses of phosphoesters by dinuclear centers: *Streptomyces* aminopeptidase as a "natural model system", *Chem. Commun.* 2501–2502.
22. DeFrank, J. J., and Cheng, T.-c. (1991) Purification and properties of an organophosphorus acid anhydrolase from a halophilic bacterial isolate, *J. Bacteriol. 173,* 1938–1943.

23. DeFrank, J. J., Beaudry, W. T., Cheng, T.-c., Harvey, S. P., Stroup, A. N., and Szafraniec, L. L. (1993) Screening of halophilic bacteria and *Alteromonas* species for organophosphorus hydrolyzing enzyme activity, *Chem.-Biol. Interact. 87*, 141−148.

24. Cheng, T.-c., Liu, L., Wang, B., Wu, J., DeFrank, J. J., Andreson, D. M., Rastogi, V. K., and Hamilton, A. B. (1997) Nucleotide sequence of a gene encoding an organophosphorus nerve agent degrading enzyme from *Alteromonas haloplanktis*, *J. Ind. Microbiol. Biotechnol. 18*, 49−55.

25. Kimura, E., and Koike, T. (1997) Intrinsic properties of zinc(II) ion pertinent to zinc enzymes, *Adv. Inorg. Chem. 44*, 229−261.

26. Kimura, E. (1994) Macrocyclic polyamine zinc(II) complexes as advanced models for zinc(II) enzymes, *Prog. Inorg. Chem. 41*, 443−491.

27. Hegg, E. L., and Burstyn, J. N. (1998) Toward the development of metal-based synthetic nucleases and peptidases: A rationale and progress report in applying the principles of coordination chemistry, *Coord. Chem. Rev. 173*, 133−165.

28. Williams, N. H., Takasaki, B., Wall, M., and Chin, J. (1999) Structure and nuclease activity of simple dinuclear metal complexes: Quantitative dissection of the role of metal ions, *Acc. Chem. Res. 32*, 485−493.

29. Vahrenkamp, H. (1999) Transitions, transition states, transition state analogues: Zinc pyrazolylborate chemistry related to zinc enzymes, *Acc. Chem. Res. 32*, 589−596.

30. Blasko, A., and Bruice, T. C. (1999) Recent studies of nucleophilic, general-acid, and metal ion catalysis of phosphate diester hydrolysis, *Acc. Chem. Res. 32*, 475−484.

31. Kimura, E. (2001) Model studies for molecular recognition of carbonic anhydrase and carboxypeptidase, *Acc. Chem. Res. 34*, 171−179.

32. Christianson, D. W., and Lipscomb, W. N. (1989) Carboxypeptidase A, *Acc. Chem. Res. 22*, 62−69.

33. Lipscomb, W. N., and Sträter, N. (1996) Recent advances in zinc enzymology, *Chem. Rev. 96*, 2375−2434.

34. Sträter, N., Lipscomb, W. N., Klabunde, T., and Krebs, B. (1996) Two-metal ion catalysis in enzymatic acyl- and phosphoryl-transfer reactions, *Angew. Chem., Int. Ed. Engl. 35*, 2024−2055.

35. Wilcox, D. E. (1996) Binuclear metallohydrolases, *Chem. Rev. 96*, 2435−2458.

36. Steinhagen, H., and Helmchem, G. (1996) Asymmetric two-center catalysis—Learning from nature, *Angew. Chem., Int. Ed. Engl. 35*, 2239−2342.

37. Fothergill, M., Goodman, M. F., Petruska, J., and Warshel, A. (1995) Structure-energy analysis of the role of metal ions in phosphoester bond hydrolysis by DNA polymerase I, *J. Chem. Am. Soc. 117*, 11619−11627.

38. Black, C. B., Huang, H.-W., and Cowan, J. A. (1994) Biological coordination chemistry of magnesium, sodium, and potassium ions—Protein and nucletide-binding sites, *Coord. Chem. Rev. 135/136*, 165−202.

39. Kim, E. E., and Wyckoff, H. W. (1991) Reaction mechanism of alkaline phosphotase based on crystal strutures—Two-metal ion catalysis, *J. Mol. Biol. 218*, 449−464.

40. Matthews, B. W. (1988) Structural basis of the action of thermolysin and related zinc peptidases, *Acc. Chem. Res. 21*, 333−340.

41. Weston, J. (2005) Mode of action of bi- and trinuclear zinc hydrolases and their synthetic analogues, *Chem. Rev. 105*, 2151−2174.

42. Greenblatt, H. M., Almog, O., Maras, B., Spungin-Bialik, A., Barra, S., Blumberg, S., and Shoham, G. (1997) *Streptomyces griseus* aminopeptidase: X-ray crystallographic structure at 1.75 Å resolution, *J. Mol. Biol. 265*, 620−636.

43. Gilboa, R., Greenblatt, H. M., Perach, M., Spungin-Bialik, A., Lessel, U., Wohlfahrt, G., Schomburg, D., Blumberg, S., and Shoham, G. (2000) Interactions of *Streptomyces griseus* aminopeptidase with a methionine product analogue: A structural study at 1.53 Å resolution, *Acta Crystallogr., Sect. D: Biol. Crystallogr. 56*, 551−558.

44. Gilboa, R., Spungin-Bialik, A., Wohlfahrt, G., Schomburg, D., Blumberg, S., and Shoham, G. (2001) Interactions of *Streptomyces griseus* aminopeptidase with amino acid reaction products and their implications toward a catalytic mechanism, *Proteins: Struct., Funct., Genet. 44*, 490−504.

45. Chevrier, B., Schalk, C., D'Orchymont, H., Rondeau, J.-M., Moras, D., and Tarnus, C. (1994) Crystal structure of *Aeromonas proteolytica* aminopeptidase—A prototypical member of the co-catalytic zinc enzyme family, *Structure 2*, 283−291.

46. Stamper, C. C., Bienvenue, D. L., Bennett, B., Ringe, D., Petsko, G. A., and Holz, R. C. (2004) Spectroscopic and X-ray crystallographic characterization of bestatin bound to the aminopeptidase from *Aeromonas (Vibrio) proteolytica*, *Biochemistry 43*, 9620−9628.

47. Stamper, C., Bennett, B., Edwards, T., Holz, R. C., Ringe, D., and Petsko, C. (2001) Inhibition of the aminopeptidase from *Aeromonas proteolytica* by L-leucinephosphonic acid. Spectroscopic and crystallographic characterization of the transition state of peptide hydrolysis, *Biochemistry 40*, 7035−7046.

48. Burley, S. K., David, P. R., Taylor, A., and Lipscomb, W. N. (1990) Leucine aminopeptidase—bestatin inhibition and a model for enzyme-catalyzed peptide hydrolysis, *Proc. Natl. Acad. Sci. U.S.A. 87*, 6878−6882.

49. Burley, S. K., David, P. R., Taylor, A., and Lipscomb, W. N. (1992) Structure determination and refinement of bovine lens leucine aminopeptidase and its complex with bestatin, *J. Mol. Biol. 224*, 113−140.

50. Roderick, S. L., and Matthews, B. W. (1993) Structure of cobalt dependent methionine aminopeptidase from *Eschericia coli*—A new type of proteolytic enzyme, *Biochemistry 32*, 3907−3912.

51. Wilce, M. C. J., Bond, C. S., Dixon, N. E., Freeman, H. C., Guss, J. M., Lilley, P. E., and Wilce, J. A. (1998) Structure and mechanism of a proline-specific aminopeptidase from *Escherichia coli*, *Proc. Natl. Acad. Sci. U.S.A. 95*, 3472−3477.

52. Graham, S. C., Lee, M., Freeman, H. C., and Guss, J. M. (2003) An orthorhombic form of *Escherichia coli* aminopeptidase P at 2.4 Å resolution, *Acta Crystallogr., Sect. D: Biol. Crystallogr. 59*, 897−902.

53. Maher, M. J., Ghosh, M., Grunden, A. M., Menon, A. L., Adams, M. W., Freeman, H. C., and Guss, J. M. (2004) Structure of the prolidase from *Pyrococcus furiosus*, *Biochemistry 43*, 2771−2783.

54. Harris, M. N., and Ming, L.-J. (1999) Different phosphate binding modes of *Streptomyces griseus* aminopeptidase between crystal and solution states and the status of zinc-bound water, *FEBS Lett. 455*, 321−324.

55. Harris, M. N., Bertolucci, C., and Ming, L.-J. (2002) Paramagnetic cobalt(II) as a probe for kinetic and NMR relaxation studies of phosphate binding and the catalytic mechanism of *Streptomyces griseus* dinuclear aminopeptidase, *Inorg. Chem. 41*, 5582−5588.

56. Sträter, N., and Lipscomb, W. N. (1995) 2-metal ion mechanism of bovine lens leucine aminopeptidase—Active-site solvent structure and binding mode of L-leucinal, *gem*-diolate transition-state analog, by X-ray crystallography, *Biochemistry 34*, 14792−14800.

57. Sträter, N., and Lipscomb, W. N. (1995) Transition state analogue L-leucinephosphonic acid bound to bovine lens leucine aminopeptidase: X-ray structure at 1.65 Å resolution in a new crystal form, *Biochemistry 34*, 9200−9210.

58. Lowther, W. T., and Matthews, B. W. (2000) Structure and function of the methionine aminopeptidases, *Biochim. Biophys. Acta 1477*, 157−167.

59. Spungin, A., and Blumberg, S. (1989) *Streptomyces griseus* aminopeptidase is a calcium-activated zinc metalloprotein—Purification and properties of the enzyme, *Eur J. Biochem. 183*, 471−477.

60. Lin, L.-Y., Park, H. I., and Ming, L.-J. (1997) Metal-binding and active-site structure of di-zinc *Streptomyces griseus* aminopeptidase, *J. Biol. Inorg. Chem. 2*, 744−749.

61. Ben-Meir, D., Spungin, A., Ashkenazi, R., and Blumberg, S. (1993) Specificity of *Streptomyces griseus* aminopeptidase and modulation of activity by metal ion binding and substitution, *Eur. J. Biochem. 212*, 107−112.

62. Brocklehurst, K., and Dixon, H. B. F. (1976) pH-dependence of the steady-state rate of a two-step enzymic reaction, *Biochem. J. 155*, 61−70.

63. Brocklehurst, K., and Dixon, H. B. F. (1977) The pH-dependence of the second-order rate contants of enzyme modification may provide free-reactant pK_a values, *Biochem. J. 167*, 859−862.

64. Harris, M. N., Madura, J. D., Ming, L.-J., and Harwood, V. J. (2001) Kinetic and mechanistic studies of the prolyl oligopeptidase from the hyperthermophile *Pyrococcus furiosus*, *J. Biol. Chem. 276*, 19310−19317.

65. Venkatasubban, K. S., and Schowen, R. L. (1986) The proton inventory technique, *CRC Crit. Rev. Biochem. 17*, 1−44.

66. Loo, S., and Erman, J. E. (1977) The rate of reaction between cytochrome C peroxidase and hydrogen peroxide is not diffusion limited, *Biochim. Biophys. Acta 481*, 279−282.

67. Brouwer, A. C., and Kirsch, J. F. (1982) Investigation of diffusion-limited rates of chymotrypsin reactions by viscosity variation, *Biochemistry 21*, 1302−1307.

68. Polgar, L., and Felfoldi, F. (1998) Oligopeptidase B: Cloning and probing stability under nonequilibrium conditions, *Proteins: Struct., Funct., Bioinf. 30*, 424−434.

69. Umezawa, H., Aoyagi, T., Suda, H., Hamada, M., and Takeuchi, T. (1976) Plipastatins: New inhibitors of phospholipase A2, produced by *Bacillus cereus* BMG302-fF67. I. Taxonomy, production, isolation and preliminary characterization, *J. Antibiot. 29*, 97−99.

70. Wilkes, S. H., and Prescott, J. M. (1985) The slow, tight binding of bestatin and amastatin to aminopeptidases, *J. Biol. Chem. 260*, 13154−13162.

71. Lejczak, B., Kafarski, P., and Zygmunt, J. (1989) Inhibition of aminopeptidases by aminophosphonates, *Biochemistry 28*, 3549−3555.

72. Chevrier, B., D'Orchymont, H., Schalk, C., Tarnus, C., and Moras, D. (1996) Structure of the *Aeromonas proteolytica* aminopeptidase complexed with a hydroxamate inhibitor. Involvement in catalysis of Glu151 and two zinc ions of the co-catalytic unit, *Eur. J. Biochem. 237*, 393−398.

73. Alberty, R. A., and Silbey, R. J. (1997) *Physical Chemistry*, 2nd ed., Chapter 11, Wiley, New York.

74. Makinen, M. W., Wells, G. B., and Kang S.-O. (1984) Structure and mechanism of carboxypeptidase A, *Adv. Inorg. Biochem. 6*, 1−70.

75. Kunuki, H., Hirohara, H., and Ise, N. (1982) pH and temprature dependences of thermolysin catalysis. Catalytic role of zinc-coordinated water, *Eur. J. Biochem. 124*, 157−163.

76. Baker, J. O., and Prescott, J. M. (1983) *Aeromonas* aminopeptidase: pH dependence and a transition-state-analogue inhibitor, *Biochemistry 22*, 5322−5331.

77. Fasman, G. D., Ed. (1975) *Handbook of Biochemistry and Molecular Biology*, 3rd ed., CRC Press, Cleaveland, OH.

78. Woolley, P. (1975) Models for metal ion function in carbonic anhydrase, *Nature 258*, 677−682.

79. Fundoiano-Hershcovitz, Y., Rabinovitch, L., Langut, Y., Reiland, V., Shoham, G., and Shoham, Y. (2004) Identification of the catalytic residues in the double-zinc aminopeptidase from *Streptomyces griseus*, *FEBS Lett. 571*, 192−196.

80. Bzymek, K. P., and Holz, R. C. (2004) The catalytic role of glutamate 151 in the leucine aminopeptidase from *Aeromonas proteolytica*, *J. Biol. Chem. 279*, 31018−31025.

81. Laidler, K. J., and Bunting, P. S. (1973) *The Chemical Kinetics of Enzyme Action*, Chapter 8, Oxford University Press, London, U.K.

82. Chen, G., Edwards, T., D'souza, V. M., and Holz, R. C. (1997) Mechanistic studies on the aminopeptidase from *Aeromonas proteolytica*: A two-metal ion mechanism for peptide hydrolysis, *Biochemistry 36*, 4278−4286.

83. Mugford, P. F., Magloire, V. P., and Kazlauskas, R. J. (2005) Unexpected subtilisin-catalyzed hydrolysis of a sulfinamide bond in preference to a carboxamide bond in *N*-acyl sulfinamides, *J. Am. Chem. Soc. 127*, 6536−6537.

84. Herschlag, D., and O'Brien, P. J. (2001) Functional interrelationships in the alkaline phosphatase superfamily: Phosphodiesterase activity of *Escherichia coli* alkaline phosphatase, *Biochemistry 40*, 5691−5699.

85. Dotson, S. B., Smith, C. E., Ling, C. S., Barry, G. F., and Kishore, G. M. (1996) Identification, characterization, and cloning of a phosphonate monoester hydrolase from *Burkholderia caryophilli* PG2982, *J. Biol. Chem. 271*, 25754−25761.

86. Shim, H., Hong, S.-B., and Raushel, F. M. (1998) Hydrolysis of phosphodiesters through transformation of the bacterial phosphotriesterase, *J. Biol. Chem. 273*, 17445−17450.

87. Kelly, J. S., Dardinger, D. E., and Butler, L. G. (1975) Hydrolysis of phosphonate esters catalyzed by 5′-nucleotide phosphodiesterase, *Biochemistry 14*, 4983−4988.

88. Kelly, J. S., and Burtler, L. G. (1975) Enzymic hydrolysis of phosphonate esters, *Biochem. Biophys. Res. Commun. 66*, 316−321.

89. Vogel, A., Schilling, O., Niecke, M., Bettmer, J., and Meyer-Klaucke, W. (2002) ElaC encodes a novel binuclear zinc phosphodiesterase, *J. Biol. Chem. 277*, 29078−29085.

90. Radzicka, A., and Wolfenden, R. (1995) A proficient enzyme, *Science 26*, 90−93.

91. Northrop, D. B. (1999) Rethinking fundamentals of enzyme action, *Adv. Enzymol. Relat. Areas Mol. Biol. 73*, 25−55.

92. O'Brien, P. J., and Herschlag, D. (1998) Sulfatase activity of *E. coli* alkaline phosphatase demonstrates a functional link to arylsulfatases, an evolutionarily related enzyme family, *J. Am. Chem. Soc. 120*, 12369−12370.

93. Takasaki, B. K., and Chin, J. (1995) La(III)-hydrogen peroxide cooperativeity in phosphate diester cleavage−A mechanistic study, *J. Am. Chem. Soc. 117*, 8582−8585.

94. Chin, J., Banaszczyk, M., Jubian, V., and Zou, X. (1989) Co(III) complex promoted hydrolysis of phosphate diesters−Comparison in reactivity of rigid *cis*-diaquotetraazacobalt(III) complexes, *J. Am. Chem. Soc. 111*, 186−190.

95. Kirby, A. J., and Younas, M. (1970) Reactivity of phosphate esters−Diester hydrolysis, *J. Chem. Soc. B 510*−513.

96. Westheimer, F. H. (1987) Why nature chose phosphates, *Science 235*, 1173−1178.

97. Kahne, D., and Still, W. C. (1988) Hydrolysis of a peptide bond in neutal water, *J. Am. Chem. Soc. 110*, 7529−7534.

98. Bond, C. S., Clements, P. R., Ashby, S. J., Collyer, C. A., Harrop, S. J., Hopwood, J. J., and Guss, J. M. (1997) Structure of a human lysosomal sulfatase, *Structure 5*, 277−289.

99. Lukatela, G., Krauss, N., Theis, K., Selmer, T., Gieselmann, V., von Figura, K., and Saenger, W. (1998) Crystal structure of human arylsulfatase A: The aldehyde function and the metal ion at the active site suggest a novel mechanism for sulfate esters hydrolysis, *Biochemistry 37*, 3654−3664.

100. Galperin, M. Y., Bairoch, A., and Koonin, E. V. (1998) A superfamily of metalloenzymes unifies phosphopentomutase and cofactor-independent phosphoglycerate mutase with alkaline phosphatases and sulfatases, *Protein Sci. 7*, 1829−1835.

101. Bender, M. L., Kézdy, F. J., and Gunter, C. R. (1964) The anatomy of an enzymatic catalysis α-chymotrypsin, *J. Am. Chem. Soc. 86*, 3714−3721.

102. Kunugi, S., Hirohara, H., and Ise, N. (1979) Kinetic and thermodynamic study of the specificity in the elementary steps of α-chymotrypsin-catalysed hydrolysis reaction, *J. Am. Chem. Soc. 101*, 3640−3646.

103. Wolfenden, R., Ridgway, C., and Young, G. (1998) Spontaneous hydrolysis of ionized phosphate monoesters and diesters and the proficiencies of phosphatases and phosphodiesterases as catalysts, *J. Am. Chem. Soc. 120*, 833−834.

104. Fry, F. H., Fischmann, A. J., Belousoff, M. J., Spiccia, L., and Brügger, J. (2005) Kinetics and mechanism of hydrolysis of a model phosphate diester by [Cu(Me3tacn)(OH2)2]2+ (Me3tacn, 1,4,7-trimethyl-1,4,7-triazacyclononane), *Inorg. Chem. 44*, 941−950.

105. Riordan, J. F. (1979) Arginyl residues and anion binding sites in proteins, *Mol. Cell. Biochem. 26*, 71−92.

106. Chueh, S. H., Chang, G. G., Chang, T. C., and Pan, F. (1981) Involvement of arginine residue in the phosphate binding site of human placental alkaline phosphatase, *Int. J. Biochem. 13*, 1143−1149.

107. Mota de Freitas, D., and Valentine, J. S. (1984) Phosphate is an inhibitor of copper−zinc superoxide dismutase, *Biochemistry 23*, 2079−2082.

108. Dahms, N. M., Rose, P. A., Molkentin, J. D., Zhang, Y., and Brzycki, M. A. (1993) The bovine mannose 6-phosphatase indulin-like growth factor-II receptor−The role of arginine residue in mannose 6-phosphate binding, *J. Biol. Chem. 268*, 5457−5463.

109. Kawase, S., Cho, S. W., Rozelle, J., Stroud, R. M., Finer-Moore, J., and Santi, D. V. (2000) Replacement set mutagenesis of the four phosphate-binding arginine residues of thymidylate synthase, *Protein Eng. 13*, 557−563.

110. Farley, R. A., Elquza, E., Muller-Ehmsen, J., Kane, D. J., Nagy, A. K., Kasho, V. N., and Faller, L. D. (2001) O18-Exchange evidence that mutations of arginine in a signature sequence for P-type pumps affect inorganic phosphate binding, *Biochemistry 6361*−6370.

111. Prager, E. M., and Wilson, A. C. (1988) Ancient origin of lactalbumin from lysozyme: Analysis of DNA and amino acid sequences, *J. Mol. Evol. 27*, 326−335.

112. Nitta, K., and Sugai, S. (1989) Evolution of lysozyme and α-lactalbumin, *Eur. J. Biochem. 182*, 111−118.

113. McKenzie, H. A., and White, F. H. (1991) Lysozyme and α-lactalbumin−Structure, function, and interrelationships, *Adv. Protein Chem. 41*, 173−315.

114. Qasba, P. K., and Kumar, S. (1997) Molecular divergence of lysozymes and α-lactalbumin, *Crit. Rev. Biochem. Mol. Biol. 32*, 255.

115. Bond, C. S., Clements, P. R., Ashby, S. J., Collyer, C. A., Harrop, S. J., Hopwood, J. J., and Guss, J. M. (1997) Structure of a human lysosomal sulfatase, *Structure 5*, 277−289.

116. Lukatela, G., Krauss, N., Theis, K., Selmer, T., Gieselmann, V., von Figura, K., and Saenger, W. (1998) Crystal structure of human arylsulfatase A: The aldehyde function and the metal ion at the active site suggest a novel mechanism for sulfate ester hydrolysis, *Biochemistry 37*, 3654−3664.

117. Bennett, M. S., Guan, Z., Laurberg, M., and Su, X. D. (2001) *Bacillus subtilis* arsenate reductase is structurally and functionally similar to low molecular weight protein tyrosine phosphatases, *Proc. Natl. Acad. Sci. U.S.A. 98*, 13577−13582.

118. Mukhopadhyay, R., Zhou, Y., and Rosen, B. P. (2003) Directed evolution of a yeast arsenate reductase into a protein−tyrosine phosphatase, *J. Biol. Chem. 278*, 24476−24480.

119. Zegers, I., Martins, J. C., Willem, R., Wyns, L., and Messens, J. (2001) Arsenate reductase from *S. aureus* plasmid pI258 is a phosphatase drafted for redox duty, *Nat. Struct. Biol. 8*, 843−847.

120. Que, L., Jr., and True, A. E. (1990) Dinuclear iron- and manganese-oxo sites in biology, *Prog. Inorg. Chem. 38*, 97−200.

121. da Silva, G. F. Z., and Ming, L.-J. (2005) Catechol oxidase activity of di-Cu^{2+}-substituted aminopeptidase from *Streptomyces griseus*, *J. Am. Chem. Soc. 127*, 16380−16381.